

QuCOOP: A Versatile Framework for Solving Composite and Binary-Parametrised Problems on Quantum Annealers

Natacha Kuete Meli¹ Vladislav Golyanik²
¹University of Siegen
www.vsa.informatik.uni-siegen.de

Marcel Seelbach Benkner¹ Michael Moeller¹
²MPI for Informatics, SIC
<https://4dqv.mpi-inf.mpg.de>

Abstract

There is growing interest in solving computer vision problems such as mesh or point set alignment using Adiabatic Quantum Computing (AQC). Unfortunately, modern experimental AQC devices such as D-Wave only support Quadratic Unconstrained Binary Optimisation (QUBO) problems, which severely limits their applicability. This paper proposes a new way to overcome this limitation and introduces QuCOOP, an optimisation framework extending the scope of AQC to composite and binary-parametrised, possibly non-quadratic problems. The key idea of QuCOOP is to iteratively approximate the original objective function by a sequel of local (intermediate) QUBO forms, whose binary parameters can be sampled on AQC devices. We experiment with quadratic assignment problems, shape matching and point set registration without knowing the correspondences in advance. Our approach achieves state-of-the-art results across multiple instances of tested problems¹.

1. Introduction

Adiabatic Quantum Computing (AQC) has become a promising approach for solving combinatorial optimisation problems in different fields of science including computer vision [3, 46, 48, 70]. AQC leverages principles of quantum mechanics to explore optimisation landscapes in a way that classical methods cannot do, allowing them to tunnel through energy barriers and escape local minima. Unfortunately, current AQC devices such as D-Wave’s machines, also referred to as *Quantum Annealers*, are restricted to *Quadratic Unconstrained Binary Optimisation (QUBO)* problems. Any deviations from the QUBO form—e.g., when the objective function is non-quadratic or quadratic in a non-linear function of the binary variables—makes the potential benefits of AQC not directly accessible. At the same time, many computer vision problems re-

¹project page: <https://4dqv.mpi-inf.mpg.de/QuCOOP/>

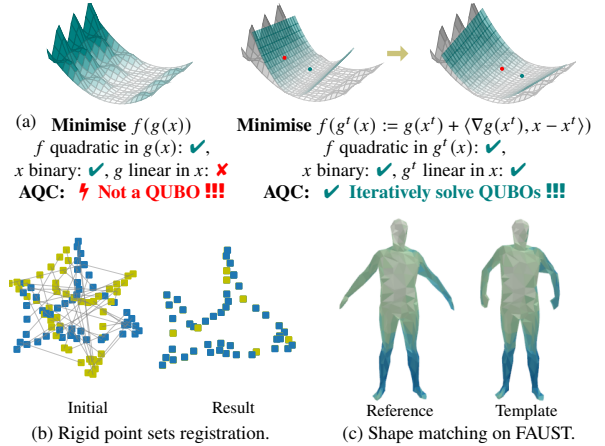


Figure 1. (a) Our QuCOOP framework for solving composite and binary-parametrised problems using Adiabatic Quantum Computing (AQC). Some qualitative results are shown for: (b) Point set registration without known correspondences; (c) Mesh alignment problems. Our general approach is competitive with specialised existing quantum and classical methods; it is compatible with quantum annealers and classical simulated annealing solvers.

quire non-quadratic objectives to obtain accurate solutions. Motivated by the tangible implications for computer vision of the restriction of the current AQC generation to QUBOs, we develop a new AQC-based optimisation method that can handle a certain type of non-quadratic objective functions.

We consider the general problem

$$\arg \min_{s \in \mathcal{S}} f(s) \quad (1)$$

of optimising a function $f : \mathcal{S} \rightarrow \mathbb{R}$ over a feasible set $\mathcal{S} \subseteq \mathbb{R}^n$. Moreover, we assume \mathcal{S} to be parameterizable by elements of a set $\mathcal{X} \subset \mathbb{R}^k$ via a smooth function $g : \mathcal{X} \rightarrow \mathcal{S}$ allowing to rewrite Problem (1) in a composite form as

$$\arg \min_{x \in \mathcal{X}} f(g(x)). \quad (2)$$

If $\mathcal{X} = \mathbb{R}^k$, Problem (2) describes an unconstrained problem and can be solved locally, or even globally (for $f \circ g$

convex in x) using gradient-based methods. If $\mathcal{X} \subsetneq \mathbb{R}^k$, Problem (2) becomes a constrained optimisation problem. If \mathcal{X} is further non-convex, as e.g., the set $\mathbb{B}^k := \{0, 1\}^k$ of binary vectors of length k , Problem (2) is generally \mathcal{NP} -hard [52] and, very often, can be solved only approximately.

Gradient descent [54, 56] is perhaps the most simple algorithm for solving Problem (2) when $\mathcal{X} = \mathbb{R}^k$. It is an iterative method, where at each iteration t , a local model f^t of f is constructed around the current iterate x^t to identify a descent direction for updating x^t . For constrained problems, one typically turns to iterative projection or additional penalty terms to ensure that all iterates x^t remain feasible. Examples of such techniques include: Gradient projection methods [7] that project the iterates of gradient descent onto \mathcal{X} ; interior-point methods [60] that minimize an augmented objective function where a so-called barrier function penalizes non-feasible iterates; feasible direction methods [59], e.g., Frank-Wolfe [28], that compute a feasible descent direction by solving an easier constrained problem and then update the iterate accordingly.

One of the strengths of AQC is its natural ability to optimize over discrete binary variables, whereas classical methods often resort to relaxations. To leverage this, we present QuCOOP (Quantum Framework for COmposite and Binary-Parametrised OPTimisation Problems), a general framework to solve (2) on AQCs. We are concerned with the case when $\mathcal{X} = \mathbb{B}^k := \{0, 1\}^k$ and f is a quadratic function in $g(x)$. The key idea is to iteratively minimize a 1D cut of f at a current *linear* Taylor approximation of g : At iteration t , we approximate f through a local model f^t by linearising the inner function g around the current iterate x^t . Since f is quadratic in $g(x)$ and x binary, the resulting sub-objectives are QUBO problems for which modern quantum annealers provide an exciting new way to sample possible low-energy states. As a result, our proposed optimisation does not require descent directions or step sizes in the usual sense as classical methods do, but directly targets a state x^{t+1} minimising f^t . See Fig. 1-(a) for an overview.

Applications. Our configuration of Problem (2) is common in computer vision. Applications we are interested in this work include the Quadratic Assignment Problem (QAP, [45]), a reputed \mathcal{NP} -hard problem that aims to optimize a quadratic function over the set of permutation matrices. QAP models many real-life problems such as graph matching [5, 6], travelling salesman [30], facility location [45], or scheduling problems [32], to name just a few. Moreover, we show in further application examples how to solve mesh alignment [6] and rigid point set registration without input correspondences [49] with QuCOOP. See Fig. 1-(b, c) for representative results.

Contributions. Our primary technical contributions are:

- QuCOOP, a new general framework for solving composite and binary-parametrised problems on AQCs (Sec. 4);
- An iterative scheme to construct and solve QUBO problems that locally approximate the original, perhaps non-quadratic objective function;
- Applications of QuCOOP to a variety of computer vision problems including QAP, shape alignment and point set registration (Secs. 5 and 6). For correspondence problems, we introduce a binary parametrisation of permutation matrices fitting in the proposed QuCOOP framework. We experimentally validated the algorithm, first with simulated annealing and achieving state-of-the-art results for several considered problems (Secs. 7.1 to 7.3); then on real D-Wave quantum annealers and improving the dimensionality of solvable permutation-related problems compared to previous quantum-compatible approaches (Sec. 7.4).

2. Related Work

Classical Optimisation Theory. A binary optimisation technique related to ours is the quadratisation of pseudo-Boolean functions [36, 47]. Pseudo-Boolean functions are functions that can be written uniquely as a multi-linear polynomial of binary variables, with QUBOs being a particular types of those with degrees not exceeding two. Quadratisation techniques [12, 47, 63] can be generally used to reduce the degree of higher-order polynomials to two in order to obtain a QUBO form. However, they often require auxiliary variables, which increases the problem size and can be costly for actual AQC devices. In contrast, QuCOOP does not require additional variables. Moreover, it is not restricted to polynomials, but could also be applied to any function as long as it fits in our composite form, see Eq. (6).

Next, our proposed QuCOOP technique falls into the class of composite optimisation methods [31, 43, 58]. These approaches leverage the composite form of optimisation problem (2) to derive easy-to-solve sub-problems that return better local optima of the original problem. An incomplete list of example applications of composite optimisation problems in computer vision include super-resolution from raw time-of-flight data [31], image and point set registration [50], shape matching [6, 16, 74]. Composite optimisation is classically well studied for continuous problems [22, 31, 43, 58]. This work explores similar techniques for the discrete case, especially to leverage AQC-based optimisation. Hence, in a broad sense, this work improves our understanding of how AQCs can be used for optimising non-quadratic objectives.

Quantum-enhanced Computer Vision (QeCV). In computer vision, AQCs have been used to solve problems such as matching involving optimising over permutation matrices [5, 6, 9]; object tracking [78] by optimising binary assignments between observations and a set of tracks; or

clustering [79] by sampling multiple binary assignments of a sample set to models its posterior distribution. Several other approaches [8, 33, 49, 68, 69] were focused on registering point sets. A feature shared by all above-mentioned methods is the construction of QUBO problems with binary solution parametrisation that suit quantum annealers.

Remark. QeCV methods relying on gate-based quantum computing remain substantially less explored than AQC [61], and many works in this domain are theoretical, heavily use simulators and are at the intersection with quantum machine learning [18, 35, 44]. One of the reasons is that quantum annealing can be considered the most advanced quantum computing technology nowadays, while fault-tolerant quantum computers that could be useful in computer vision are under development [1].

The IQT Approach [49]. The most closely related work to ours is the iterative quantum transformation (IQT) approach of Kuete Meli *et al.* [49]. IQT iteratively finds rotation matrices R aligning two point sets using AQC. Since rotations can be parametrised by non-redundant parameters v (e.g., a rotation angle in 2D and rotation angle and axis in 3D), the original constrained problem on rotation matrices is cast in Ref. [49] into an unconstrained optimisation problem over rotation parameters. Specifically, IQT iteratively linearizes R around a current rotation parameter as $R(v) = R(v^t) + \langle \nabla R(v^t), v - v^t \rangle + \mathcal{O}(\|v - v^t\|^2)$ and uses an AQC to sample, in each iteration, a binary representation of v minimising a target function quadratic in $R(v)$. Hence, the IQT approach can be interpreted as a special case of QuCOOP, i.e., a more general optimisation technique relying on AQC as will become apparent from Sec. 4.

3. Background

As our method is designed for AQC devices, we briefly revise their principles. We also review classical composite optimisation, which QuCOOP builds upon. For a detailed introduction to quantum computing and numerical optimisation, see Ref. [20, 55, 71] and [54, 56], respectively.

3.1. Adiabatic Quantum Computing

Adiabatic Quantum Computing (AQC) is a model of quantum computation which is polynomially equivalent to the circuit model [2]. *Quantum annealers* (QAs) are experimental realisations of the AQC paradigm that do not perfectly fulfill the adiabaticity condition [3, 20, 38, 48]. They provide a meta-heuristic for finding globally-optimal solutions to combinatorial optimisation problems relying on the evolution of a quantum-mechanical system driven by quantum fluctuations. Usually they optimize QUBO objectives, i.e., problems of the form

$$\arg \min_{x \in \mathbb{B}^k} \langle x, \mathbf{Q}x + \mathbf{c} \rangle, \quad (3)$$

where $\langle \cdot, \cdot \rangle$ is the standard inner product in \mathbb{R}^k , \mathbf{Q} a symmetric matrix, and \mathbf{c} a vector. QUBO problems are \mathcal{NP} -hard in general, and solving them on a QA is of high practical interest. Casting computer vision problems to QUBO forms can be challenging and has become an active research area [6, 9, 79]. While QUBOs can be optimised with classical optimisation techniques such as *Simulated Annealing (SA)* [41], QA is expected to offer substantial advantages over SA in certain cases [20, 21].

In QA, the provided QUBO problem is converted to the corresponding physical Ising *Hamiltonian* \mathbf{H}_p . The mapping is such that the ground state of \mathbf{H}_p , i.e. the spin configuration of the physical system achieving the minimal energy value, encodes the solution of the QUBO. To obtain the ground state of \mathbf{H}_p , the system evolves according to a time-dependent *Hamiltonian* $\mathbf{H}(t)$ changing from the initial Hamiltonian \mathbf{H}_i (with a known ground state) to \mathbf{H}_p , e.g. in the way that $\mathbf{H}(t) = (1 - \frac{t}{T})\mathbf{H}_i + t\mathbf{H}_p$ for $t \in [0, T]$. If the system transitions according to the adiabatic theorem of quantum mechanics [11, 37, 39] it stays always in a ground state. One of the conditions is a slow-enough transition, e.g. a one that is inversely proportional to the squared minimum (over all instantaneous t) *spectral gap* of \mathbf{H} . In practice, modern experimental realisations of AQCs are non-adiabatic and return ground states with probabilities $\ll 1.0$. To increase the probability of finding the ground state at least once, annealing is repeated multiple times.

3.2. Composite Optimisation

Iterative methods [54, 56] solve Problem (2) by repeatedly minimising a local model f^t built upon the actual iterate x^t :

$$x^{t+1} := \arg \min_{x \in \mathcal{X}} f^t(x), \quad (4)$$

where the local model f^t should have some nice properties such as convexity or separability making it easier to solve.

In *composite optimisation*, also known as ‘prox-linear’ or ‘prox-descent’ [22, 31, 43, 58], the idea is to exploit the underlying composite nature of the objective function in Problem (2) to derive a local model that, still being easier to solve, approximates the original landscape more faithfully. Two approaches to achieve this are to either approximate the outer function f [31], or linearize the inner function g [22, 43, 58]. In the later case, the local model reads

$$f^t(x) := f(g(x^t) + \langle \nabla g(x^t), x - x^t \rangle) + \frac{1}{2\alpha^t} \|x - x^t\|_2^2, \quad (5)$$

with α^t being the step size that prevents x^{t+1} to deviate too much from x^t , point around which the approximation is more reliable. It is shown in Ref. [58] that for a convex and coercive f and under the Kurdyka–Łojasiewicz-property, the iterates $(x^t)_{t=1}^\infty$ for the model Eq. (5) converge

to a critical point, *i.e.* a minimizer of f . We build on this later approximation, *i.e.* the linearisation of the inner function g , to derive QUBOs for AQC, as we consider that the outer function f is quadratic in $g(x)$.

4. The Proposed QuCOOP Iteration

This section describes our general QuCOOP framework, followed by its applications in Sec. 5 and Sec. 6. Proofs of all Lemmas are given in Appendix A.

QuCOOP is an optimisation algorithm for composite optimisation problems of the form (2), where f is quadratic in $g(x)$, that iteratively uses AQC. The function $g : \mathbb{R}^k \rightarrow \mathbb{R}^n$ is a smooth function such that $\mathcal{S} = \text{Im}_g(\mathbb{B}^k) := \{g(x) : x \in \mathbb{B}^k\}$, hence, g parametrizes the feasible domain $\mathcal{S} \subsetneq \mathbb{R}^n$ of the original Problem (1) by elements of the set $\mathcal{X} := \mathbb{B}^k$. For convenience, we write Problem (1) as

$$f(g(x)) = \langle g(x), \mathbf{Q}g(x) + \mathbf{c} \rangle, \quad (6)$$

for a given matrix $\mathbf{Q} \in \mathbb{R}^{n \times n}$ and a vector $\mathbf{c} \in \mathbb{R}^n$.

Note that for Problem (1), we are only interested in values of g on \mathbb{B}^k . However, from a theoretical point of view, our algorithm involves a Taylor approximation of g , requiring g to be smooth as described above. Such a g is far from being unique. Moreover, in addition to $\mathcal{S} = \text{Im}_g(\mathbb{B}^k)$, the gradient of g can take any value by design. Thus, from a practical point of view, this function g should model a “reasonable” or “natural” smooth parametrisation of \mathcal{S} .

A high-level description of the algorithm is provided in Algorithm 1. Next, we analyse its different steps.

Algorithm 1: QuCOOP Iteration

Initialize x^0 and repeat for $t = 0, 1, 2, \dots$

$$g^t(x) := g(x^t) + \langle \nabla g(x^t), x - x^t \rangle \quad (7)$$

$$x^{t+1} \leftarrow \arg \min_{x \in \mathbb{B}^k} \{f^t(x) := f(g^t(x))\} \quad (8)$$

s.t. $g^t(x) \in \mathcal{S}$

Return $g(x^{t+1})$.

The first step is the familiar choice of the starting point x^0 . This can be a vector based on prior knowledge, the result of a previous optimisation, or any random point. As will be discussed later in Lemma 1, QuCOOP converges globally, but not necessarily to the global optimum. Hence, different x^0 can lead to different results.

In a subsequent loop, at each iteration t , the inner function g is linearised around the current iterate x^t using first-order Taylor expansion, Eq. (7), and the next iterate x^{t+1} is computed by solving the minimisation Problem (8). Evaluated on the hyperplane $g^t(x)$, f results in a

k -dimensional quadratic function f^t in variable x . In cases where the parametrisation $g^t(x)$ differs substantially from the parametrisation $g(x)$, to guarantee a monotone decrease of the objective values, it might also be necessary to include a step $x^{t+1} = g^{-1}(g^t(\tilde{x}^{t+1}))$, with \tilde{x} being the output of Problem (8).

Fig. 1 provides a visual intuition of the constructed local model f^t . Next, we ensure the compatibility of Problem (8) with quantum annealers (see Sec. 3.1) through a QUBO formulation.

The Unconstrained Part of Problem (8). The objective function of the minimisation in Problem (8) is already in an AQC-compatible form. At iteration t , we solve the QUBO

$$\arg \min_{x \in \mathcal{X}} \langle x, \mathbf{Q}^t x + \mathbf{c}^t \rangle, \quad \text{with} \quad (9)$$

$$\mathbf{Q}^t := \nabla g(x^t) \mathbf{Q} \nabla g(x^t)^\top, \quad (10)$$

$$\mathbf{c}^t := \nabla g(x^t) \left(\mathbf{c} + 2\mathbf{Q} \left(g(x^t) - \nabla g(x^t)^\top x^t \right) \right). \quad (11)$$

This is because the local model f^t now becomes quadratic in the binary variable x . Details on the derivation of this QUBO problem can be found in Appendix B.

Meeting the Constraint of Problem (8). In classical optimisation when \mathcal{X} is convex, *cf.* Eq. (5), the damping term factored to the step size ensures that $g(x)$ or x remains close to $g(x^t)$ or x^t . This is reminiscent of trust-region methods requiring that the local model f^t trustfully approximates f , which happens in a close neighborhood of x^t .

In our case, \mathcal{X} is discrete, but the quantum annealer can essentially navigate the complete \mathcal{X} domain, allowing us to explore solutions beyond the trust region. At the same time, as required in Problem (8), we have to guarantee that $g^t(x) \in \mathcal{S}$; or, more generally, to replace it with a nearby feasible point with the objective value not much worse than the linearised estimate $f(g^t(x))$. As the whole QuCOOP iteration should be carried out by AQC, ensuring this feasibility amounts to designing a penalty term in the form of a quadratic function in $g^t(x)$. Depending on the form of \mathcal{S} , this may, or may not, be easy computationally. The yet resulting objective function is a standard QUBO problem that can run on AQC. We refer to Secs. 5 and 6 for exemplary penalty functions on two computer vision problems, namely graph or shape matching and point set registration.

Convergence Analysis. While QuCOOP does not guarantee global convergence, it, at least, monotonically decreases the objective function values as stated next:

Lemma 1. *The series $(f(g(x^t)))_{t \in \mathbb{N}}$ generated by Algorithm 1 with reparametrisation, or without and under assumptions found in Appendix A, monotonically decreases.*

5. Graph Matching and QAP with QuCOOP

This section shows an application of QuCOOP to graph matching and quadratic assignment problems (QAP).

A general graph matching problem of size $n \in \mathbb{N}$ can be written in matrix form as

$$\arg \min_{\mathbf{P} \in \Pi_n} \|\mathbf{A}\mathbf{P} - \mathbf{P}\mathbf{B}\|_F^2, \quad (12)$$

where \mathbf{A} and \mathbf{B} are given $n \times n$ symmetric matrices and Π_n is the set of all $n \times n$ permutation matrices [16]. Equivalently, by assuming the constraint $\mathbf{P} \in \Pi_n$ to be always held and ignoring resulting constant terms, Eq. (12) becomes

$$\arg \min_{\mathbf{P} \in \Pi_n} -\langle \mathbf{A}\mathbf{P}, \mathbf{P}\mathbf{B} \rangle_F. \quad (13)$$

The Quadratic Assignment Problem (QAP) aims to maximize (13). To apply QuCOOP to (13), we need to parametrise the permutation matrix \mathbf{P} using binary variables:

Lemma 2. *Let $((a, b), a, b = 1, \dots, n, a < b)$, with cardinality $k := n(n-1)/2$, be the tuple of all 2-cycles permuting a and b , and \mathbf{T}_i the matrix representation of the i -th cycle. Any permutation matrix can be parametrised with a length- k binary vector $x := (x_1, \dots, x_k)$ via the function*

$$\mathbf{P} : \mathbb{B}^k \rightarrow \Pi_n$$

$$x \mapsto \mathbf{P}(x) := \prod_{i=1}^k \mathbf{P}_i(x_i), \quad \mathbf{P}_i(x_i) := \mathbf{T}_i^{x_i}, \quad (14)$$

where $\mathbf{T}_i^{x_i}$ is \mathbf{T}_i if $x_i = 1$ and the identity $\mathbf{I}_{n \times n}$ otherwise.

Next, we construct out of \mathbf{P} from Eq. (14) a smooth function g to be used in QuCOOP. A natural choice is to design, for each \mathbf{P}_i from Eq. (14), a smooth function defined through $\mathbf{P}_i(x_i) = x_i(\mathbf{T}_i - \mathbf{I}_n) + \mathbf{I}_n$ for $x_i \in \mathbb{R}$, which makes \mathbf{P}_i and thus \mathbf{P} differentiable with respect to x_i and thus x . Now letting $g(x) := \mathbf{p}(x) := \text{vec}(\mathbf{P}(x))$ be the vector formed by the rows of $\mathbf{P}(x)$, we propose to solve Problem (13) using Algorithm 1 by solving at each iteration t the sub-problem

$$\arg \min_{x \in \mathcal{X}} \langle g^t(x), \mathbf{Q}g^t(x) \rangle, \quad \mathbf{Q} := \alpha \mathbf{I}_{n \times n} - \mathbf{A} \otimes \mathbf{B}, \quad (15)$$

where $g^t(x) = \mathbf{p}^t(x) = \mathbf{p}(x^t) + \langle \nabla \mathbf{p}(x^t), x - x^t \rangle$. The term $\alpha \mathbf{I}_{n \times n}$ is, for some $\alpha \in \mathbb{R}_+$, the penalty added to enforce $\mathbf{p}^t(x) \in \Pi_n$ as required by QuCOOP. In the next paragraph, we justify why our penalty term effectively penalizes non-feasible solutions. Finally, the optimisation follows Algorithm 1 with $x \in \mathcal{X} = \mathbb{B}^k$.

On the Penalty Term of the Permutation Constraint.

We next show why minimising $\alpha \|\mathbf{p}^t(x)\|_2^2$ effectively constrains the result of the minimisation step in (15) to lie in the set Π_n of permutation matrices. At iteration t , we have

$$\mathbf{p}^t(x) = \mathbf{p}(x^t) + \langle \nabla \mathbf{p}(x^t), x - x^t \rangle, \quad (16)$$

in which each row of $\nabla \mathbf{p}(x^t)$, that is, each partial derivative of \mathbf{p} (cf. Eq. (42) in the supplement), contains exactly two 1 and two -1 entries. A following nice property of QuCOOP is that its iterates $\mathbf{P}^t(x)$ partially satisfy the permutation matrix constraint in the sense that their rows and columns sum up to ones, as stated in Lemma 3.

Lemma 3. *All the iterates $\mathbf{P}^t(x)$ computed by Algorithm 1 for $\mathbf{P}(x)$ from Eq. (14) fulfill $\mathbf{P}^t(x) \in X, \forall x \in \mathbb{B}^k$, where*

$$X := \left\{ \mathbf{M} \in \mathbb{Z}^{n \times n} \mid \sum_{i=1}^n \mathbf{M}_{ij} = \sum_{j=1}^n \mathbf{M}_{ij} = 1, \forall ij \right\}. \quad (17)$$

As a consequence of Lemma 3, $n \leq \|\mathbf{p}^t(x)\|_2^2$ holds so that minimising $\|\mathbf{p}^t(x)\|_2^2$ enforces $\mathbf{P}^t(x) \in \Pi_n$ as desired.

6. Point Set Registration with QuCOOP

We next apply QuCOOP to point set registration. Given a reference set $\mathbf{X} := (x_i)_{i=1}^n \in \mathbb{R}^{d \times n}$ and a template set $\mathbf{Y} := (y_i)_{i=1}^n \in \mathbb{R}^{d \times n}$, our goal is to determine the best rotation $\mathbf{R} \in \text{SO}(d)$ and the best permutation $\mathbf{P} \in \Pi_n$ that jointly transform the template set and find correspondences with the reference set. Concretely, we aim to solve

$$\arg \min_{\mathbf{R} \in \text{SO}(d), \mathbf{P} \in \Pi} \|\mathbf{X}\mathbf{P} - \mathbf{R}\mathbf{Y}\|_F^2. \quad (18)$$

By assuming the constraints $\mathbf{R} \in \text{SO}(d)$ and $\mathbf{P} \in \Pi_n$ to be always fulfilled and discarding resulting constant terms, we retrieve the problem formulation:

$$\arg \min_{\mathbf{R} \in \text{SO}(d), \mathbf{P} \in \Pi} -\langle \mathbf{X}\mathbf{P}, \mathbf{R}\mathbf{Y} \rangle_F. \quad (19)$$

As required by Algorithm 1, we need to binary-parametrise \mathbf{R} and \mathbf{P} . For \mathbf{P} , we use the parametrisation from Lemma 2, again with a total of $k_p := n(n-1)/2$ binary parameters. For \mathbf{R} , we follow Ref. [33, 49] and write \mathbf{R} using the exponential mapping from the orthogonal Lie algebra to its group, as a function $\mathbf{R}(y) = \exp(\mathbf{M}(y))$, where \mathbf{M} is a skew-symmetric matrix depending on the rotation parameter $y \in \mathbb{R}^k$, with $k_r := d(d-1)/2$.

By flattening the optimisation variables $\mathbf{R}(y)$ and $\mathbf{P}(x)$ as $\mathbf{r}(y) := \text{vec}(\mathbf{R}(y))$ and $\mathbf{p}(x) := \text{vec}(\mathbf{P}(x))$ our optimisation sub-problem in the QuCOOP iteration t becomes

$$\arg \min_{(x,y) \in \mathcal{X}} \langle g^t(x,y), \mathbf{Q}g^t(x,y) \rangle, \quad (20)$$

$$\mathbf{Q} := \begin{pmatrix} \alpha \mathbf{I}_{n \times n} & -\frac{1}{2} \mathbf{X} \otimes \mathbf{Y} \\ -\frac{1}{2} (\mathbf{X} \otimes \mathbf{Y})^\top & \beta \mathbf{I}_{d \times d} \end{pmatrix}, \quad (21)$$

where $g^t(x, y) := (\mathbf{p}^t(x), \mathbf{r}^t(y))$ with the linearisation $\mathbf{p}^t(x) = \mathbf{p}(x^t) + \langle \nabla \mathbf{p}(x^t), x - x^t \rangle$ for the permutation and $\mathbf{r}^t(y) = \mathbf{r}(y^t) + \langle \nabla \mathbf{r}(y^t), y - y^t \rangle$ for the rotation. The term $\alpha \mathbf{I}_{n \times n}$ ensures that the iterate $\mathbf{P}^t(x)$ is a valid permutation matrix, and $\beta \mathbf{I}_{d \times d}$ that $\mathbf{R}^t(y)$ approaches an orthonormal matrix. The optimisation now follows Alg. 1 in which the permutation variable x lies in \mathbb{B}^k , and, as in Ref. [49], we binarize the rotation variable y by considering its flexible m -bits discretisation over a tunable interval, leading to $y \in \mathbb{B}^{m \cdot k}$. In total, (x, y) is a binary vector in $\mathbb{B}^{k+m \cdot k}$.

7. Experimental Evaluation

We perform numerical experiments on QAP, shape matching and point set registration problems. Secs. 7.1 to 7.3 report results of our method when optimised using Simulated Annealing (SA) on classical hardware, and Sec. 7.4 reports results of the same experiments using real D-Wave Quantum Annealer (QA). Details about the used datasets and benchmark methods are discussed in the corresponding sections. SA, along with the preparation of couplings and biases of QuCOOP for the quantum annealer, is carried out on a conventional computer (AMD Ryzen 9 5900X 12-Core Processor CPU with 128GB RAM).

Penalty Factors. Similar to many other AQC methods dealing with constrained problems [5, 9, 46], our approach is not exempt from the choice of the penalty factors α in (15), and α and β in (21). The penalty factors should be large enough to enforce the constraint while not significantly worsening the dynamic range of the resulting problem Hamiltonian, which otherwise could lead to incorrect solutions of the QUBO problem on the quantum annealer [51]. In our experiments, we set the penalty factors for QAP and point set registration by grid search on smaller problems, which is a widely used approach in the field [9, 27]. In the following, α is set for QAPs to the lowest eigenvalue for $\mathbf{A} \otimes \mathbf{B}$; for shape matching problems, α is ten times the lowest eigenvalue of $\mathbf{A} \otimes \mathbf{B}$; and in point set registration, α equals $\|\mathbf{X}\|_F^2$ and β equals $0.1 \cdot \|\mathbf{Y}\|_F^2$.

7.1. Quadratic Assignment Problems (QAP)

To benchmark our method on QAP, we consider the Fast Approximate Quadratic programming for graph matching (FAQ) [75] and the 2-OPT method [19] as classical competitors, and Q-Match [6] as an AQC-compatible competitor. Implementations for FAQ and 2-OPT are provided within Python’s Scipy-library, and our method as well as Q-Match are optimised using the SA implementation provided by D-Wave. Q-Match’s source code is publicly available [4]. A technical comparison between QuCOOP and Q-Match can be found in Appendix C.

We report results on the QAPLIB dataset [15] for all instances with problem size $n \leq 50$, 72 in total. Details

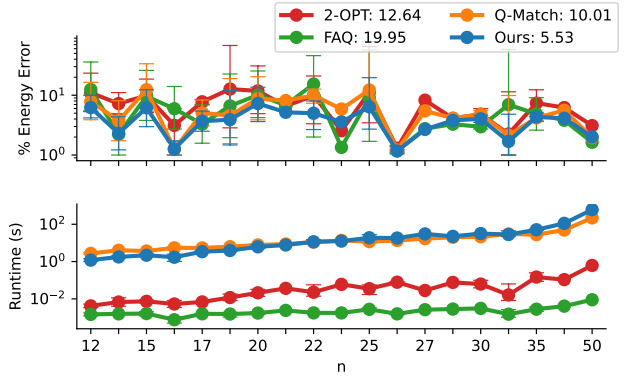


Figure 2. Benchmark results on QAPLIB [15]. We plot the percentage energy error for all considered problem instances (note the means over all instances reported in the legend) and provide their runtimes. Our method clearly outperforms its competitors.

on those problem instances, along with calculated objective values, are provided in the supplement, Tab. III. Fig. 2 shows the relative errors of the computed objective values w.r.t. optimal ones. Overall, our method consistently outperforms both classical and quantum competitors and has the smallest confidence intervals. Our method and Q-Match exhibit higher runtimes compared to FAQ and 2-Opt for almost all n . This can be explained by the fact that Q-Match solves smaller problems but requires a lot of iterations (≈ 800 for $n = 50$), while QuCOOP solves larger problems in much fewer iterations (≈ 5 for $n = 50$).

7.2. Shape Matching

We match pairs $(\mathcal{U}, \mathcal{V})$ of reduced meshes from the FAUST dataset [10], with 502 vertices each following Seelbach Benkner *et al.* [6]. We follow Ref. [6] in several further design choices. Due to the high problem dimensionality, we break down each problem into carefully selected sub-problems solved iteratively. An initial registration based on descriptor similarities is first calculated using linear assignment. Subsequently, in each iteration and for each vertex $u \in \mathcal{U}$, we compute the contribution $\sum_{v \in \mathcal{V}} \mathbf{Q}_{u \cdot n + \mathbf{P}_{u \cdot v \cdot n + \mathbf{P}_v}}$ to the objective function, where \mathbf{P} is the current solution. The $n = 40$ vertices with the highest mismatch scores on both meshes are selected as sub-meshes and registered using either our QuCOOP or Q-Match [6] to enhance registration. We repeat until the set of worst vertices converges.

The evaluation metric is the common Princeton benchmark protocol [40] which calculates for each $u \in \mathcal{U}$ the geodesic distance between the computed and the optimal vertex assignment of u , normalised by the diameter of \mathcal{V} . We report cumulative geodesic errors, *i.e.* the percentage of assignments with error below incremental thresholds.

Fig. 3 displays some qualitative registration results and Fig. 4 presents the function value decrease over the iter-

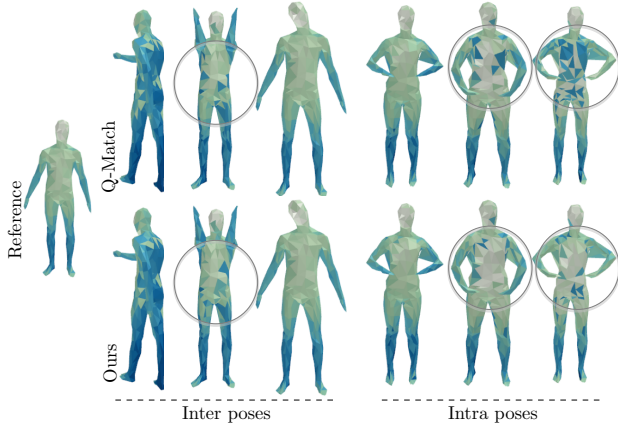


Figure 3. Registration results on FAUST [10]. The proposed approach performs at least as well as Q-Match [6]; see circled areas.

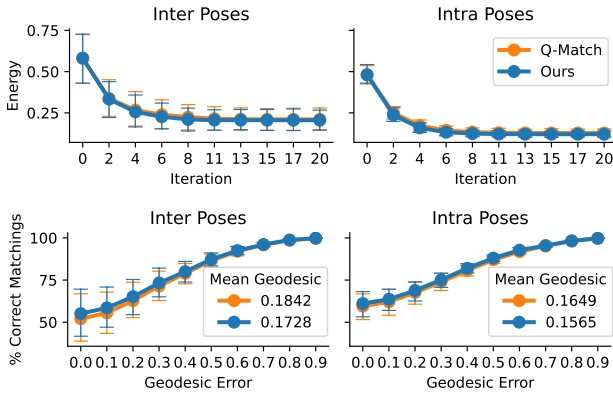


Figure 4. Energy decrease and geodesic errors, averaged on ten instances of FAUST [10] in each pose category. The mean geodesic error for both methods is given in the legend of the plot. The proposed method performs slightly better than Q-Match [6].

ations as well as the cumulative geodesic errors. Failure cases are discussed in Appendix E. Our general QuCOOP framework clearly matches the accuracy of the previous specialised Q-Match method. It reduces the mean geodesic error by about 0.01, as it can achieve better results on the sub-problems (see Appendix C). This selection of worst vertices, however, also worsens the performance of both methods, preventing them from matching the results of recent classical state-of-the-art methods [64, 65, 80].

7.3. Point Set Registration

We perform experiments on 2D and 3D point set registration. In 2D, points were picked on fish images, and in 3D they were generated from geometrical curves. The number of points varies from $n = 20$ to $n = 40$. We benchmark QuCOOP against the classical rigid CPD algorithm [53] implemented within the pycpd package [29]. Quantum com-

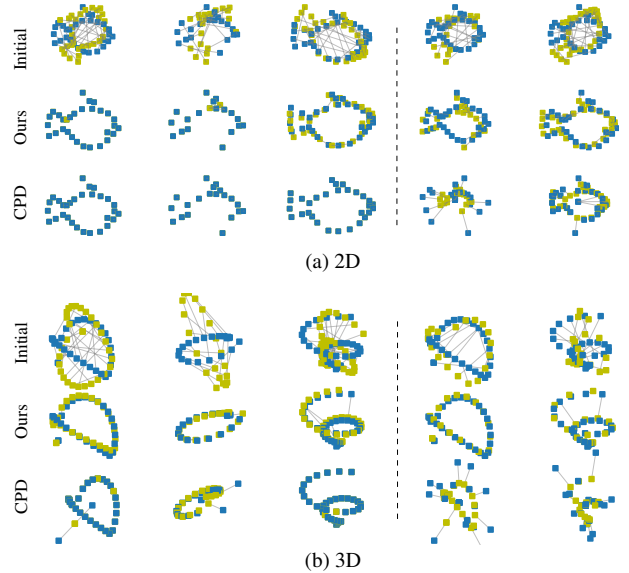


Figure 5. Registration results on 2D and 3D point sets with different n . Grey lines show correspondences between reference (olive) and template (blue) points. With up to a few correspondence errors, our method performs well on both isomorphic (left to vertical line) and non-isomorphic shapes (right to vertical line). CPD performs better on isomorphic shapes than on non-isomorphic shapes.

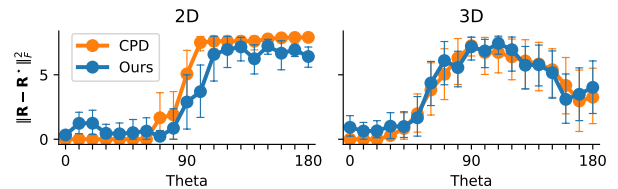


Figure 6. Varying rotation angle in the point sets registration experiment. Both CPD and our method show difficulties to register the points for a rotation angle exceeding 90° in 2D and 45° in 3D.

petitor methods that would have been IQT [49] and QA [33] cannot handle registration without correspondences.

Fig. 5 shows our registration results. Left to the vertical line in the figure are point sets that are isomorphic up to the rotation and permutation, Right are cases where, additionally, the sets are non-isomorphic and/or have different number of points. In the later case, we zero-pad the set with the lowest cardinality to match the other. We use $k_r = 10$ variables for the rotation parameter and perform 15 iterations on each problem instance. We see that QuCOOP’s computed correspondences are overall correct, so that a reasonable transformation of the template set can still be found. CPD shows difficulties in registering non-isomorphic sets.

In Fig. 6, we show registration performances, averaged over ten random problem instances of size $n = 10$, for both methods, while varying the rotation angle. The larger the rotation angle, the harder the registration for both methods.

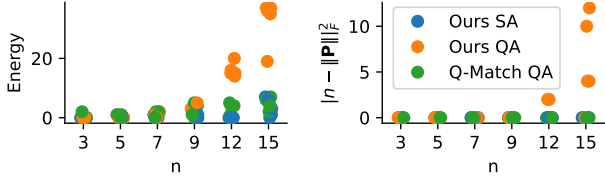


Figure 7. D-Wave results for 5 randomly generated QAP instances for $n = 3, 5, 7, 9, 12, 15$. Left are returned energy function values, 0 being the best. Right is the validness $|n - \|\mathbf{P}\|_F^2|$ of returned matrices, 0 indicating a valid permutation matrix. Up to $n \approx 12$, D-Wave finds valid permutation matrices, and often optimal ones.

7.4. Experiments on D-Wave Machines

We now execute QuCOOP on a real quantum device, D-Wave Advantage 6.4 accessed through the Leap API [23–25]. Advantage has >5000 physical qubits connected in the Pegasus topology. However, due to the connectivity pattern of the physical qubits which induces chains in the problem embedding, it is estimated that it can solve problems of about 180 fully connected logical variables, limiting our experiments to problems of sizes $n \approx 15$; see also Appendix G.

QAP. On D-Wave, we solve 5 randomly generated QAP instances for $n = 3, 5, 7, 9, 12, 15$. The entries of matrix \mathbf{A} are $\mathbf{A}_{ij} = \|x_i - x_j\|_2$ for standard and normally distributed $\{x_i \in \mathbb{R}^2\}_{i=1}^n$, and \mathbf{B} equals $\mathbf{P}^\top \mathbf{A} \mathbf{P}$ such that, according to Eq. (12), the optimal function value is 0. Each iteration of the algorithm is executed with the default annealing time of $20\mu\text{s}$ and 50 sample reads. We investigate, whether the last computed matrices (*i.e.* $\mathbf{P} = \mathbf{P}^t(x^{t+1})$) are valid permutation matrices² and plot their function values. We compare against the SA implementation and Q-Match (with QA).

Our results are reported in Fig. 7. Up to $n \approx 12$, QuCOOP QA finds valid permutation matrices, but returns higher objective values compared to QuCOOP SA and Q-Match QA. As n becomes large, QuCOOP QA tends to compute non-valid matrices. QuCOOP QA took about $5 \times$ less runtime than Q-Match QA on one problem instance, including overheads such as minor embedding and access. Compared to previous works [5, 77] which reasonably—*i.e.* by returning valid permutation matrices—solved only problems of size $n = 3, 4$ on D-Wave machines, we consider QuCOOP as an improvement of the state-of-the-art.

Point Set Registration. We perform point set registration on D-Wave for five randomly generated problem instances for $n = 3, 5, 7, 9, 12, 15$ in each set. The results are reported in Fig. 8. Qualitative results can be found in Appendix F. We see that QuCOOP can register the points without correspondences up to $n = 5$, improving previous work [49] in which correspondences are known beforehand.

²Note that $\mathbf{P}^t(x^{t+1})$ may be non-valid, but $\mathbf{P}(x^{t+1})$ is always valid.

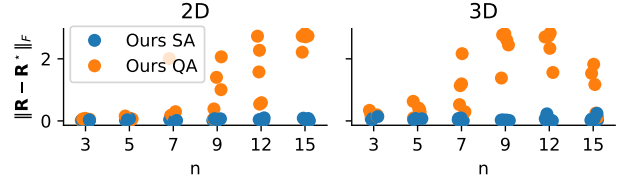


Figure 8. D-Wave results for five randomly generated point sets registrations for $n = 3, 5, 7, 9, 12, 15$. In line with the QAP experiment, D-Wave successfully registers small problem instances.

8. Discussion and Limitations

The experiments reveal several features of QuCOOP: First, its ability to handle problems involving permutation problems; second, its versatility and compatibility with continuous problems such as point set registration without correspondences, which previous techniques [6, 33, 49] are not able to address. Moreover, QuCOOP supports optimisation over permutation matrices up to size $n=12$ using the chosen parametrisation on D-Wave annealers.

Approximation Accuracy. As for many first-order methods, the linearisation g^t of the inner function g is both the key and the bottleneck of QuCOOP. It may not always provide accurate approximations for highly non-linear g and lead to suboptimal solutions as observed in the tests.

Scalability and Scaling. The space complexity of our permutation parameterisation scales quadratically with n , making it difficult to solve large problems on D-Wave, as complex embeddings increase the chain break probability.

9. Conclusion

We have presented QuCOOP, a framework for solving composite, binary-parametrised and possibly non-quadratic problems using AQC. This represents a new class of problems solvable on AQC previously restricted to QUBO forms. QuCOOP solves a sequence of QUBO forms approximating the original objective function, which facilitates the non-intuitive and challenging task of handcrafting QUBOs for the aforementioned problem types. We show that our single framework can effectively be applied to several computer vision problems. Namely, we address QAP and shape matching problems, outperforming the previous specialised quantum-enhanced Q-Match method by 5% on QAP and 0.01 on shape matching. For the first time, an AQC-compatible method for rigid point set registration is shown not to require input correspondences and match the accuracy of the classical CPD algorithm on tested problems. We hope this work inspires future exploration of new methods for other CV problems within the proposed framework.

Acknowledgements

This work was supported by the Deutsche Forschungsgemeinschaft (DFG, German Research Foundation), project number 534951134.

References

- [1] Rajeev Acharya et al. Quantum error correction below the surface code threshold. *arXiv*, 2024. 3
- [2] Dorit Aharonov, Wim Van Dam, Julia Kempe, Zeph Landau, Seth Lloyd, and Oded Regev. Adiabatic quantum computation is equivalent to standard quantum computation. *SIAM review*, 50(4):755–787, 2008. 3
- [3] Tameem Albash and Daniel A. Lidar. Adiabatic quantum computation. *Reviews of Modern Physics*, 90(1), 2018. 1, 3
- [4] Marcel Seelbach Benkner. Source Code of Q-Match. github.com/MSeelbach/Q-Match, 2021. 6
- [5] Marcel Seelbach Benkner, Vladislav Golyanik, Christian Theobalt, and Michael Moeller. Adiabatic quantum graph matching with permutation matrix constraints. In *International Conference on 3D Vision (3DV)*, 2020. 2, 6, 8
- [6] Marcel Seelbach Benkner, Zorah Löhner, Vladislav Golyanik, Christof Wunderlich, Christian Theobalt, and Michael Moeller. Q-match: Iterative shape matching via quantum annealing. In *International Conference on Computer Vision*, pages 7586–7596, 2021. 2, 3, 6, 7, 8, 4
- [7] Dimitri P Bertsekas. On the goldstein-levitin-polyak gradient projection method. *IEEE Transactions on automatic control*, 21(2):174–184, 1976. 2
- [8] Harshil Bhatia, Edith Tretschk, Zorah Löhner, Marcel Seelbach Benkner, Michael Möller, Christian Theobalt, and Vladislav Golyanik. Ccuantumm: Cycle-consistent quantum-hybrid matching of multiple shapes. In *Computer Vision and Pattern Recognition (CVPR)*, 2023. 3
- [9] Tolga Birdal, Vladislav Golyanik, Christian Theobalt, and Leonidas J Guibas. Quantum permutation synchronization. In *Computer Vision and Pattern Recognition (CVPR)*, pages 13122–13133, 2021. 2, 3, 6
- [10] Federica Bogo, Javier Romero, Matthew Loper, and Michael J Black. Faust: Dataset and evaluation for 3d mesh registration. In *Computer Vision and Pattern Recognition (CVPR)*, pages 3794–3801, 2014. 6, 7
- [11] Max Born and Vladimir Fock. Beweis des adiabatenatzes. *Zeitschrift für Physik*, 51(3-4):165–180, 1928. 3
- [12] Endre Boros and Aritanan Gruber. On quadratization of pseudo-boolean functions. *arXiv*, 2014. 2
- [13] Alexander M Bronstein, Michael M Bronstein, and Ron Kimmel. *Numerical geometry of non-rigid shapes*. Springer Science & Business Media, 2008. 7, 9
- [14] Rainer E Burkard and Josef Offermann. Entwurf von schreibmaschinentastaturen mittels quadratischer zuordnungsprobleme. *Zeitschrift für Operations Research*, 21: B121–B132, 1977. 8
- [15] Rainer E Burkard, Stefan E Karisch, and Franz Rendl. Qaplib—a quadratic assignment problem library. *Global optimization*, 10:391–403, 1997. 6, 7
- [16] Rainer E Burkard, Eranda Cela, Panos M Pardalos, and Leonidas S Pitsoulis. *The quadratic assignment problem*. Springer, 1998. 2, 5
- [17] Nicos Christofides and Enrique Benavent. An exact algorithm for the quadratic assignment problem on a tree. *Operations Research*, 37(5):760–768, 1989. 8
- [18] Iris Cong, Soonwon Choi, and Mikhail D Lukin. Quantum convolutional neural networks. *Nature Physics*, 15(12): 1273–1278, 2019. 3
- [19] Georges A Croes. A method for solving traveling-salesman problems. *Operations research*, 6(6):791–812, 1958. 6
- [20] Arnab Das and Bikas K Chakrabarti. *Quantum annealing and related optimization methods*. Springer Science & Business Media, 2005. 3
- [21] Vasil S Denchev, Sergio Boixo, Sergei V Isakov, Nan Ding, Ryan Babbush, Vadim Smelyanskiy, John Martinis, and Hartmut Neven. What is the computational value of finite-range tunneling? *Physical Review X*, 6(3):031015, 2016. 3
- [22] Dmitriy Drusvyatskiy and Courtney Paquette. Efficiency of minimizing compositions of convex functions and smooth maps. *Mathematical Programming*, 178:503–558, 2019. 2, 3
- [23] D-Wave Systems. QPU Solver Datasheet. https://docs.dwavesys.com/docs/latest/doc_qpu.html, 2024. 8
- [24] D-Wave Systems. D-Wave Leap. <https://www.dwavesys.com/take-leap>, 2024.
- [25] D-Wave Systems. D-Wave Ocean Software Documentation. <https://docs.ocean.dwavesys.com/>, 2024. 8
- [26] Bernhard Eschermann and Hans-Joachim Wunderlich. A unified approach for the synthesis of self-testable finite state machines. In *Design Automation Conference*, page 372–377, New York, NY, USA, 1991. 8
- [27] Matteo Farina, Luca Magri, Willi Menapace, Elisa Ricci, Vladislav Golyanik, and Federica Arrigoni. Quantum multi-model fitting. In *Computer Vision and Pattern Recognition (CVPR)*, 2023. 6
- [28] Marguerite Frank, Philip Wolfe, et al. An algorithm for quadratic programming. *Naval research logistics quarterly*, 3(1-2):95–110, 1956. 2
- [29] Anthony A Gatti et al. Pure numpy implementation of the coherent point drift algorithm. <https://github.com/siavashk/pycpd>, 2022. 7
- [30] Bezalel Gavish and Stephen C Graves. The travelling salesman problem and related problems. 1978. 2
- [31] Jonas Geiping and Michael Moeller. Composite optimization by nonconvex majorization-minimization. *SIAM Journal on Imaging Sciences*, 11(4):2494–2528, 2018. 2, 3
- [32] Arthur M Geoffrion and Glenn W Graves. Scheduling parallel production lines with changeover costs: Practical application of a quadratic assignment/lp approach. *Operations Research*, 24(4):595–610, 1976. 2
- [33] Vladislav Golyanik and Christian Theobalt. A quantum computational approach to correspondence problems on point sets. In *Computer Vision and Pattern Recognition (CVPR)*, pages 9182–9191, 2020. 3, 5, 7, 8

- [34] Scott W Hadley, Franz Rendl, and Henry Wolkowicz. A new lower bound via projection for the quadratic assignment problem. *Mathematics of Operations Research*, 17(3):727–739, 1992. 8
- [35] Tak Hur, Leeseok Kim, and Daniel K Park. Quantum convolutional neural network for classical data classification. *Quantum Machine Intelligence*, 4(1):3, 2022. 3
- [36] Hiroshi Ishikawa. Higher-order clique reduction in binary graph cut. In *Computer Vision and Pattern Recognition (CVPR)*, pages 2993–3000, 2009. 2
- [37] Sabine Jansen, Mary-Beth Ruskai, and Ruedi Seiler. Bounds for the adiabatic approximation with applications to quantum computation. *Mathematical Physics*, 48(10):102111, 2007. 3
- [38] Tadashi Kadowaki and Hidetoshi Nishimori. Quantum annealing in the transverse Ising model. *Phys. Rev. E*, 58:5355–5363, 1998. 3
- [39] Tosio Kato. On the adiabatic theorem of quantum mechanics. *The Physical Society of Japan*, 5(6):435–439, 1950. 3
- [40] Vladimir G Kim, Yaron Lipman, and Thomas Funkhouser. Blended intrinsic maps. *ACM transactions on graphics (TOG)*, 30(4):1–12, 2011. 6
- [41] Scott Kirkpatrick, C Daniel Gelatt Jr, and Mario P Vecchi. Optimization by simulated annealing. *science*, 220(4598):671–680, 1983. 3
- [42] Jakob Krarup and Peter Mark Pruzan. Computer-aided layout design. *Mathematical programming in use*, pages 75–94, 1978. 8
- [43] Adrian S Lewis and Stephen J Wright. A proximal method for composite minimization. *Mathematical Programming*, 158:501–546, 2016. 2, 3
- [44] YaoChong Li, Ri-Gui Zhou, RuQing Xu, Jia Luo, and Wen-Wen Hu. A quantum deep convolutional neural network for image recognition. *Quantum Science and Technology*, 5(4):044003, 2020. 3
- [45] Eliane Maria Loiola, Nair Maria Maia De Abreu, Paulo Oswaldo Boaventura-Netto, Peter Hahn, and Tania Querido. A survey for the quadratic assignment problem. *European journal of operational research*, 176(2):657–690, 2007. 2
- [46] Andrew Lucas. Ising formulations of many np problems. *Frontiers in physics*, 2:74887, 2014. 1, 6
- [47] Avradip Mandal, Arnab Roy, Sarvagya Upadhyay, and Hayato Ushijima-Mwesigwa. Compressed quadratization of higher order binary optimization problems. In *Computing Frontiers*, pages 126–131, 2020. 2
- [48] Catherine C McGeoch. *Adiabatic quantum computation and quantum annealing: Theory and practice*. Morgan & Claypool Publishers, 2014. 1, 3
- [49] Natacha Kuete Meli, Florian Mannel, and Jan Lellmann. An iterative quantum approach for transformation estimation from point sets. In *Computer Vision and Pattern Recognition (CVPR)*, pages 529–537, 2022. 2, 3, 5, 6, 7, 8
- [50] Jan Modersitzki. *FAIR: flexible algorithms for image registration*. SIAM, 2009. 2
- [51] Sascha Mücke, Thore Gerlach, and Nico Piatkowski. Optimum-preserving qubo parameter compression. *Quantum Machine Intelligence*, 7(1):1–18, 2025. 6
- [52] Katta G Murty and Santosh N Kabadi. Some np-complete problems in quadratic and nonlinear programming. Technical report, 1985. 2
- [53] Andriy Myronenko and Xubo Song. Point set registration: Coherent point drift. *PAMI*, 32(12):2262–2275, 2010. 7
- [54] Yurii Nesterov et al. *Lectures on convex optimization*. Springer, 2018. 2, 3
- [55] Michael A. Nielsen and Isaac L. Chuang. *Quantum Computation and Quantum Information*. Cambridge University Press, Cambridge, 10th edition, 2010. 3
- [56] Jorge Nocedal and Stephen J Wright. *Numerical optimization*. Springer, 1999. 2, 3
- [57] Christopher E Nugent, Thomas E Vollmann, and John Ruml. An experimental comparison of techniques for the assignment of facilities to locations. *Operations research*, 16(1):150–173, 1968. 8
- [58] Edouard Pauwels. The value function approach to convergence analysis in composite optimization. *Operations Research Letters*, 44(6):790–795, 2016. 2, 3
- [59] Sebastian Pokutta. The frank-wolfe algorithm: a short introduction. *Jahresbericht der Deutschen Mathematiker-Vereinigung*, 126(1):3–35, 2024. 2
- [60] Florian A Potra and Stephen J Wright. Interior-point methods. *Computational and applied mathematics*, 124(1-2):281–302, 2000. 2
- [61] Lakshika Rathi, Edith Tretschk, Christian Theobalt, Rishabh Dabral, and Vladislav Golyanik. 3D-QAE: Fully quantum auto-encoding of 3d point clouds. In *British Machine Vision Conference (BMVC)*, 2023. 3
- [62] Ralph Tyrell Rockafellar. *Convex analysis:(pms-28)*. 2015. 2
- [63] Elisabeth Rodriguez Heck. *Linear and quadratic reformulations of nonlinear optimization problems in binary variables*. PhD thesis, 2018. 2
- [64] Paul Roetzer and Florian Bernard. Spidermatch: 3d shape matching with global optimality and geometric consistency. In *Computer Vision and Pattern Recognition (CVPR)*, pages 14543–14553, 2024. 7
- [65] Paul Roetzer, Paul Swoboda, Daniel Cremers, and Florian Bernard. A scalable combinatorial solver for elastic geometrically consistent 3d shape matching. In *Computer Vision and Pattern Recognition (CVPR)*, pages 428–438, 2022. 7
- [66] Catherine Roucairol. *Du séquentiel au parallèle: La recherche arborescente et son application à la programmation quadratique en variables 0.1*. PhD thesis, Éditeur inconnu, 1987. 8
- [67] Michael Scriabin and Roger C Vergin. Comparison of computer algorithms and visual based methods for plant layout. *Management Science*, 22(2):172–181, 1975. 8
- [68] Marcel Seelbach Benkner, Vladislav Golyanik, Christian Theobalt, and Michael Moeller. Adiabatic quantum graph matching with permutation matrix constraints. In *International Conference on 3D Vision (3DV)*, 2020. 3
- [69] Marcel Seelbach Benkner, Maximilian Krahn, Edith Tretschk, Zorah Lähner, Michael Moeller, and Vladislav Golyanik. Quant: Quantum annealing with learnt couplings. In *International Conference on Learning Representations (ICLR)*, 2023. 3

- [70] Peter W Shor. Polynomial-time algorithms for prime factorization and discrete logarithms on a quantum computer. *SIAM review*, 41(2):303–332, 1999. 1
- [71] Robert S Sutor. *Dancing with Qubits: How quantum computing works and how it can change the world*. Packt Publishing Ltd, 2019. 3
- [72] Éric Taillard. Robust taboo search for the quadratic assignment problem. *Parallel computing*, 17(4-5):443–455, 1991. 8
- [73] Eric D Taillard. Comparison of iterative searches for the quadratic assignment problem. *Location science*, 3(2):87–105, 1995. 8
- [74] Oliver Van Kaick, Hao Zhang, Ghassan Hamarneh, and Daniel Cohen-Or. A survey on shape correspondence. In *Computer graphics forum*, pages 1681–1707, 2011. 2
- [75] Joshua T Vogelstein, John M Conroy, Vince Lyzinski, Louis J Podrazik, Steven G Kratzer, Eric T Harley, Donniell E Fishkind, R Jacob Vogelstein, and Carey E Priebe. Fast approximate quadratic programming for graph matching. *PLOS one*, 10(4):e0121002, 2015. 6, 7
- [76] Mickey R Wilhelm and Thomas L Ward. Solving quadratic assignment problems by ‘simulated annealing’. *IIE transactions*, 19(1):107–119, 1987. 8
- [77] Alp Yurtsever, Tolga Birdal, and Vladislav Golyanik. Q-fw: A hybrid classical-quantum frank-wolfe for quadratic binary optimization. In *European Conference on Computer Vision (ECCV)*, 2022. 8
- [78] Jan-Nico Zaech, Alexander Liniger, Martin Danelljan, Dengxin Dai, and Luc Van Gool. Adiabatic quantum computing for multi object tracking. In *Computer Vision and Pattern Recognition (CVPR)*, pages 8811–8822, 2022. 2
- [79] Jan-Nico Zaech, Martin Danelljan, Tolga Birdal, and Luc Van Gool. Probabilistic sampling of balanced k-means using adiabatic quantum computing. In *Computer Vision and Pattern Recognition (CVPR)*, pages 26191–26201, 2024. 3
- [80] Aleksei Zhuravlev, Zorah Löhner, and Vladislav Golyanik. Denoising functional maps: Diffusion models for shape correspondence. In *Computer Vision and Pattern Recognition (CVPR)*, 2025. 7

QuCOOP: A Versatile Framework for Solving Composite and Binary-Parametrised Problems on Quantum Annealers

Supplementary Material

This supplementary material provides a deeper analysis of the proposed optimisation framework and more experimental details and results. It includes the following sections:

- Proofs of Lemmas 1 to 3 claimed in Sec. 4 of the main text (Appendix A);
- Details of the derivation of QuCOOP’s QUBO problem (9) of the main text (Appendix B);
- A technical comparison between our QuCOOP method and the Q-Match algorithm in solving permutation problems, as mentioned in Secs. 7.1 and 7.2 of the main text (Appendix C);
- Details on the QALIB results in Sec. 7.1 of the main text, as well as an investigation of the performance of an iterative local search variant of QuCOOP on QALIB problems (Appendix D);
- Further experiments on shape matching from Sec. 7.2 of the main text, including failure cases on FAUST and results on the TOSCA dataset (Appendix E);
- Qualitative results of point set registration computed on D-Wave complementing the numerical results of Sec. 7.4 of the main text (Appendix F);
- Description of the annealing and embedding process on D-Wave’s quantum annealers, relevant for the results in Sec. 7.4 of the main text (Appendix G).

The notation in this supplement mostly follows the conventions of the main text. We summarise them in Tab. I.

Symbol	Meaning
$\mathcal{S} \subseteq \mathbb{R}^n$	Feasible domain of an optimisation problem of interest
$\mathcal{X} = \mathbb{B}^k$	Parameter set for the feasible domain \mathcal{S}
g^t	Linear Taylor approximation of g around iterate x^t
f^t	Local model, quadratic in g^t
∇g	Gradient of g with respect to x
$\langle \cdot, \cdot \rangle$	Standard inner product in \mathbb{R}^k

Table I. Main notations used in this paper and their meaning.

A. Proofs of the Lemmas

Proof of Lemma 1. We show that the series of objective function values computed by QuCOOP is non-increasing in either of the following cases:

1. With no reparametrisation step and under following assumptions:

- The constraint $g^t(x) \in \mathcal{S}$ is enforced with a penalty term of the form $\alpha^t h(x, x^t)$ with sufficiently large penalty factor $\alpha^t \in \mathbb{R}_+$ and a function h such that $h(x^t, x^t) = 0$, and $h(x, x^t) > 0$ for all $x \neq x^t$.
- At points $g^t(x)$ in \mathcal{S} that the algorithm can reach in a specific iteration, the linearised parametrisation g^t coincides with g , so that $g^t(x^{t+1}) = g(x^{t+1})$.

2. Alternatively with the reparametrisation step:

It is always possible to change Algorithm 1 to a non-increasing algorithm by including, as mentioned in the main text, a step $x^{t+1} = g^{-1}(g^t(\tilde{x}^{t+1}))$, where \tilde{x} is the output of Problem (8).

Proof. 1. **With no reparametrisation step:**

Using Assumptions i): Majorisation-Minimisation argument:

We want to show that $f(g(x^{t+1})) \leq f(g(x^t))$ for all t .

According to the assumption in i) the Problem (8) can be explicitly written without constraint as

$$x^{t+1} \leftarrow \arg \min_{x \in \mathbb{B}} f^t(x), \quad f^t(x) := f(g^t(x)) + \alpha^t h(x, x^t), \quad (22)$$

where $\alpha^t \in \mathbb{R}_{>0}$ is a penalty factor and h some function in x ensuring the feasibility so that $g^t(x) \in \mathcal{S}$. At iteration t , the QUBO solver finds the minimiser x^{t+1} of f^t among all $x \in \mathcal{X}$ with $g^t(x) \in \mathcal{S}$. Automatically, we have $f^t(x^{t+1}) \leq f^t(x^t) = f(g(x^t))$. It remains to show that

$$f(g(x^{t+1})) \leq f^t(x^{t+1}). \quad (23)$$

We will first show that Eq. (23) can be established for specific designs of h making f^t a majoriser of $f \circ g$. More specifically, we will establish the proof for two local models $f_i^t(x) := f(g^t(x)) + \alpha^t h_i(x)$, $i = 1, 2$, with

$$h_1(x, x^t) = \langle x - x^t, \mathbf{H}(x - x^t) \rangle \quad (24)$$

$$h_2(x, x^t) = \langle g^t(x) - g(x^t), \mathbf{H}(g^t(x) - g(x^t)) \rangle, \quad (25)$$

where $\mathbf{H} \in \mathbb{R}^{k \times k}$ is some positive definite matrix ensuring the feasibility on \mathcal{S} . As a side note, the design choice h_2 is a special case of h_1 with an iteration dependent \mathbf{H}^t . To see this, we plug the expression $g^t(x) = g(x^t) + \langle \nabla g(x^t), x - x^t \rangle$ into h_2 , yielding $h_2(x, x^t) = \langle \nabla g(x^t)^\top (x - x^t), \mathbf{H} \nabla g(x^t)^\top (x - x^t) \rangle$, from which we can read out that $\mathbf{H}^t = \nabla g(x^t) \mathbf{H} \nabla g(x^t)^\top$. Note that Assumptions i) require $\nabla g(x^t)$ to have full rank, because otherwise $h_2(x, x^t)$ may be zero for $x \neq x^t$.

We now show that for h being either h_1 or h_2 , our local model f^t in Eq. (22) is a majoriser of $f \circ g$ and Eq. (23) holds. The proof follows the same argumentation as well-known Majorisation-Minimisation methods [58, Lemma 2.1 & Theorem 2.2]. In essence, from the smoothness of g , we know from [54, Lemma 1.2.3] that there exists a Lipschitz constant $a \in \mathbb{R}$ such that for all $x \in \mathbb{B}^k$ it holds

$$\|g(x) - g(x^t) - \langle \nabla g(x^t), x - x^t \rangle\|_2 \leq a \|x - x^t\|_2^2. \quad (26)$$

On the other hand, the quadratic function f is Lipschitz continuous on the finite and bounded set \mathcal{S} [62, Theorem 10.4], i.e. $\forall x, y \in \mathcal{S}$ we can find $b \in \mathbb{R}$ such that

$$|f(x) - f(y)| \leq b \|x - y\|_2. \quad (27)$$

Substituting $x = g(x)$ and $y = g^t(x)$ in Eq. (27) and using the relation in Eq. (26), we get

$$|f(g(x)) - f(g^t(x))| \leq b \|g(x) - g^t(x)\| \quad (28)$$

$$\leq ab \|x - x^t\|_2^2, \quad (29)$$

from which follows

$$f(g(x)) \leq f(g^t(x)) + ab \|x - x^t\|_2^2. \quad (30)$$

Next, we compare the objective in Eqs. (22) and (30). Given that \mathbf{H} is positive definite, it becomes clear that we can find a positive constant α^t and further majorise (30) by f_1^t as

$$f(g(x)) \leq f(g^t(x)) + ab \|x - x^t\|_2^2 \quad (31)$$

$$\leq f(g^t(x)) + \alpha^t \langle (x - x^t), \mathbf{H}(x - x^t) \rangle = f_1^t(x). \quad (32)$$

This is also true for h_2 . Since \mathbf{H} is positive definite and $\nabla g(x^t)$ has full rank, it follows that $\nabla g(x^t) \mathbf{H} \nabla g(x^t)^\top$ is positive definite too. Hence, with a proper choice of α^t , we can further majorise (30) by f_2 as

$$f(g(x)) \leq f(g^t(x)) + ab \|x - x^t\|_2^2 \quad (33)$$

$$\leq f(g^t(x)) + \alpha^t \langle \nabla g(x^t)^\top (x - x^t), \mathbf{H} \nabla g(x^t)^\top (x - x^t) \rangle = f_2^t(x). \quad (34)$$

Hence, by properly setting the penalty factor α^t we can majorise the true objective. Thus, $f(g(x)) \leq f^t(x)$ for all $x \in \mathbb{B}^k$, and specifically $f(g(x^{t+1})) + \alpha \langle g(x^t), \mathbf{H}g(x^t) \rangle \leq f^t(x^{t+1})$ as desired. Looking back at the argumentation so far we notice that we never had to use any properties of $h_2(x, x^t)$ besides the properties listed in assumption i). The assumption that $h(x^t, x^t) = 0$ is crucial to obtain $f^t(x^t) = f(g(x^t))$. The second condition that $h(x, x^t) > 0$ for all $x \neq x^t$ is important to prove that f^t is a majoriser of $f \circ g$ if α_t is chosen big enough. The general form of the inequalities (32) and (34) is

$$f(g(x)) \leq f(g^t(x)) + ab \|x - x^t\|_2^2 \quad (35)$$

$$\leq f(g^t(x)) + \alpha^t h(x, x^t) = f^t(x). \quad (36)$$

We can find values for α^t so that this holds, because $h(x, x^t)$ is non-zero for $x \neq x^t$ and since we only consider binary vectors for x and x^t . For arbitrary x with $x \neq x^t$ the function $h(x, x^t)$ could still have approached zero in some limit.

Proof using Assumption ii): Local search argument: Since QuCOOP optimizes over binary vectors x for which $g^t(x) \in \mathcal{S}$, it follows that g and g^t are both valid, possibly different parametrisations of a subset of the feasible set \mathcal{S} , and that we have found a better point on \mathcal{S} than $g(x^t)$. If the parametrisation on that point differ so that $g(x^{t+1}) \neq g^t(x^{t+1})$ it is not clear why $g(x^{t+1})$ should also have a better objective value than $g(x^t)$. However if $g(x^{t+1}) = g^t(x^{t+1})$ on all the relevant binary vectors x^t so that $g^t(x^{t+1}) \in \mathcal{S}$ we have the guarantee that $g(x^{t+1})$ has also a better energy than $g(x^t)$.

2. With the reparametrisation step:

In the case that the two parametrisations g^t and g differ, as explained in the main text, we can call \tilde{x} the output of the minimisation step in Problem (8) and re-calibrate the iterate as $x^{t+1} = g^{-1}(g^t(\tilde{x}^{t+1}))$. It follows that $f(g(x^{t+1})) \leq f(g^t(x^t)) = f(g(x^t))$ as desired. \square

Note that the re-calibration is also common in classical composite optimisation, cf. [58, Composite Gauss–Newton]. In our shape matching and point sets registration problems for the case of permutation matrices, if the iteration step stays inside the set of permutation matrices, then our linearised parametrisation g^t coincides with the original parametrisation g . We will present proof for this result later in this supplement, Lemma 5. This observation saved us the recalibration step and allowed for fast convergence. In the experiments, we also noticed a monotone decrease in the objective function values.

Proof of Lemma 2. We show that any permutation matrix \mathbf{P} of n elements can be written as an ordered product of $k = n(n-1)/2$ binary-parametrised transpositions \mathbf{P}_i .

Proof. Let \mathbf{P} be an arbitrary permutation we want to decompose in this way and let c be the cycle notation of \mathbf{P} . It is well known that any c can be written as a decomposition of disjoint cycles:

$$c = \prod_j f^{(j)}. \quad (37)$$

We will first prove that an arbitrary cycle can be written as a decomposition in 2-cycles in a fixed order. As the order for the 2-cycles we will w.l.o.g. use

$$((1, 2), (1, 3), \dots, (1, n), (2, 3), (2, 4), \dots, (n-1, n)). \quad (38)$$

The elements of the ℓ -cycle we want to decompose are denoted as

$$g = (g_1, g_2, \dots, g_\ell). \quad (39)$$

We construct the decomposition in an iterative fashion. First, let m be the index of the minimal number in the cycle so that

$$g_m = \min\{g_1, \dots, g_\ell\}. \quad (40)$$

The following identity holds for permutations:

$$(g_1, g_2, \dots, g_\ell) = (g_m g_{m+1})(g_{m+2}, g_{m+3}, \dots, g_\ell, g_1, \dots, g_{m-1}, g_{m+1}). \quad (41)$$

One notices that the problem is reduced to finding the decomposition for a $(\ell-1)$ -cycle with a minimal element bigger than g_m . Therefore one can repeat the procedure and the 2-cycles will be in the order given by Eq. (38).

The decomposition (39) only uses the elements g_1, g_2, \dots, g_ℓ . We can now find these decompositions for each of the disjoint cycles $f^{(j)}$ that c is decomposed into. Since all the cycles $f^{(j)}$ are disjoint, the 2-cycles a cycle $f^{(i)}$ is decomposed into are disjoint from the 2-cycles a cycle $f^{(j)}$ is decomposed into for $i \neq j$. Since these 2-cycles are disjoint, the product commutes and can be rearranged in the order of Eq. (38). If one has another order of the cycles than the one in Eq. (38), one also has to apply the identity (41) in a way that the final decomposition is in that order.

Finally, the number $k = n(n-1)/2$ of distinct cycles c can be decomposed into is obvious from Eq. (38). \square

We have also confirmed via computation that removing a single 2-cycle from the tuple of possible 2-cycles applied in a fixed order results in not reaching the complete $S(d)$ at least for $d \leq 6$.

Proof of Lemma 3. We show that the linear approximate permutation matrices $\mathbf{P}^t(x)$ computed by our algorithm fulfil the row and column sum to 1.

Proof. Each partial derivative of \mathbf{P} can be calculated as

$$\frac{\partial}{\partial x_i} \mathbf{P}(x) = \prod_{j=1}^{i-1} \mathbf{P}_j(x_j) \frac{\partial}{\partial x_i} \mathbf{P}_i(x_i) \prod_{j=i+1}^k \mathbf{P}_j(x_j) \quad (42)$$

with $\frac{\partial}{\partial x} \mathbf{P}_i(x_i) = \mathbf{T}_i - \mathbf{I}$. So, it is easy to see that there are exactly two rows and two columns of $\frac{\partial}{\partial x} \mathbf{P}(x)$ that are non-zero and contain exactly one 1 and one -1 each. Thus, for all $x \in \mathbb{B}^k$, it holds

$$\sum_{i=1}^n \langle \nabla \mathbf{P}(x^t), x - x^t \rangle_{ij} = 0 \quad \forall j \quad (43)$$

$$\sum_{j=1}^n \langle \nabla \mathbf{P}(x^t), x - x^t \rangle_{ij} = 0 \quad \forall i. \quad (44)$$

As per definition $\mathbf{P}^t(x) = \mathbf{P}(x^t) + \langle \nabla \mathbf{P}(x^t), x - x^t \rangle$, and since $\mathbf{P}(x^t) \in \Pi_n$ fulfils the row and column sum to 1, the validity of the claim for \mathbf{P}^t is immediate. \square

B. QUBO Derivation for QuCOOP

We provide details of the derivation of the QUBO in Eq. (9). For ease of notation, let us first write $g^t(x)$ as

$$g^t(x) = g(x^t) + \langle \nabla g(x^t), x - x^t \rangle \quad (45)$$

$$= \underbrace{g(x^t) - \nabla g(x^t)^\top x^t}_{=:g} + \underbrace{\nabla g(x^t)^\top x}_{=:g}. \quad (46)$$

Now, we have

$$f^t(x) = f(g^t(x)) \quad (47)$$

$$= \langle g_c + g_x, \mathbf{Q}(g_c + g_x) + \mathbf{c} \rangle \quad (48)$$

$$= (g_c + g_x)^\top \mathbf{Q}(g_c + g_x) + (g_c + g_x)^\top \mathbf{c} \quad (49)$$

$$= g_c^\top \mathbf{Q} g_c + 2g_x^\top \mathbf{Q} g_c + g_x^\top \mathbf{Q} g_x + g_c^\top \mathbf{c} + g_x^\top \mathbf{c} \quad (50)$$

$$= g_x^\top \mathbf{Q} g_x + g_x^\top (\mathbf{c} + 2\mathbf{Q} g_c) + g_c^\top \mathbf{Q} g_c + g_c^\top \mathbf{c}, \quad (51)$$

where the last two terms are independent with respect to the variable x . Now taking the arg min and discarding those independent terms, we obtain

$$\arg \min_{x \in \mathcal{X}} f^t(x) = \arg \min_{x \in \mathcal{X}} g_x^\top \mathbf{Q} g_x + g_x^\top (\mathbf{c} + 2\mathbf{Q} g_c), \quad (52)$$

from which we can read out the coupling matrix \mathbf{Q}^t and bias vector \mathbf{c} of the QUBO in Eq. (9).

C. Comparison against Q-Match

An interesting question is how does QuCOOP differs from Q-Match [6] on permutation problems. In Q-Match, one linearizes the inner function by selecting a set of disjoint cycles over which the optimisation is performed. For disjoint cycles, the permutation matrix can be written as a linear function of the binary variables. As formalised is Lemma 4, we observed that with our linearisation $\mathbf{P}^t(x) = \mathbf{P}(x^t) + \langle \nabla \mathbf{P}(x^t), x - x^t \rangle$ and since $\mathbf{P}(x^t) \in \Pi_n$, the minimisers x are precisely those such that $x - x^t$ selects the partial derivatives of disjoint cycles in $\nabla \mathbf{P}(x^t)$, non-disjoint cycles leading to $\mathbf{P}^t(x)$ with higher Frobenius norms that are being penalised. However, unlike Q-Match where the selection of disjoint cycles is done by hand which may be sub-optimal, our algorithm optimally selects the best set of disjoint cycles and optimises over them. We will now give the exact characterisation which permutation matrices can be obtained with our linearisation.

Characterisation of Reachable Valid Permutations

Lemma 4. *The matrix \mathbf{P}^{t+1} obtained from \mathbf{P}^t with QuCOOP is a permutation matrix, if and only if for all indices where x^t differs from x^{t+1} the conjugations of the cycles $\mathbf{T}_i^{(-1)}$ of the form*

$$C_i := \left(\prod_{j=1}^{i-1} \mathbf{T}_j^x \right) \mathbf{T}_i^{(-1)} \left(\prod_{j=i-1}^1 (\mathbf{T}_j^x)^{-1} \right) \quad (53)$$

are disjoint.

Proof. First we observe that if we start at the identity permutation the linearisation only lands on a valid permutation if disjoint cycles are applied. Later the statement will be generalised in the above way for arbitrary x^t . The linearisation can be written in general as

$$\mathbf{P}^{t+1}(x) = \mathbf{P}^t + \sum_i (x_i - x_i^t) \frac{\partial}{\partial x_i} \mathbf{P}(x)|_{x=x^t} (\mathbf{T}_i - \mathbf{I}) \prod_{j=i+1}^k \mathbf{P}_j(x_j^t) \quad (54)$$

$$= \prod_{j=1}^k \mathbf{T}_j^x + \sum_i (x_i - x_i^t) \left(\prod_{j=1}^{i-1} \mathbf{T}_j^x \right) (\mathbf{T}_i - \mathbf{I}) \prod_{j=i+1}^k \mathbf{T}_j^x. \quad (55)$$

Now we insert the zero vector for x^t . This yields $\mathbf{P}^{t+1}(x) = \mathbf{I} + \sum_i (x_i) (\mathbf{T}_i - \mathbf{I})$. Furthermore, we observe that $\mathbf{T}_i - \mathbf{I}$ has -1 as entries on the diagonal on places where the cycle \mathbf{T}_i acts non-trivially. If two cycles that are chosen are not disjoint then one adds a -2 to a diagonal element of \mathbf{I} . Therefore, we can not obtain a permutation matrix in this case.

To generalise this idea we look at the general case described in Eq. (55) and divide by \mathbf{P}^t :

$$\left(\prod_{j=1}^k \mathbf{T}_j^x \right) (\mathbf{P}^t)^{-1} = \mathbf{I} + \sum_i (x_i - x_i^t) \left(\prod_{j=1}^{i-1} \mathbf{T}_j^x \right) (\mathbf{T}_i - \mathbf{I}) \left(\prod_{j=i+1}^k \mathbf{T}_j^x \right) \left(\prod_{j=k}^1 (\mathbf{T}_j^x)^{-1} \right), \quad (56)$$

where the product symbol $\prod_{j=k}^1$ indicates that we want to apply the cycles in the reverse order than before. Note that the left side of the equation is only a permutation matrix if \mathbf{P}^{t+1} is a permutation matrix. The right side can be further simplified:

$$\left(\prod_{j=1}^k \mathbf{T}_j^x \right) (\mathbf{P}^t)^{-1} = \mathbf{I} + \sum_i (x_i - x_i^t) \left(\prod_{j=1}^{i-1} \mathbf{T}_j^x \right) (\mathbf{T}_i - \mathbf{I}) \left(\prod_{j=i}^1 (\mathbf{T}_j^x)^{-1} \right) \quad (57)$$

$$= \mathbf{I} + \sum_i (x_i - x_i^t) \left(\prod_{j=1}^{i-1} \mathbf{T}_j^x \right) (\mathbf{T}_i - \mathbf{I}) (\mathbf{T}_i^x)^{-1} \left(\prod_{j=i-1}^1 (\mathbf{T}_j^x)^{-1} \right) \quad (58)$$

$$= \mathbf{I} + \sum_i (x_i - x_i^t) \left(\prod_{j=1}^{i-1} \mathbf{T}_j^x \right) (\mathbf{T}_i^{1-x} - (\mathbf{T}_i^x)^{-1}) \left(\prod_{j=i-1}^1 (\mathbf{T}_j^x)^{-1} \right) \quad (59)$$

$$= \mathbf{I} + \sum_i (x_i - x_i^t) (-1)^x \left(\prod_{j=1}^{i-1} \mathbf{T}_j^x \right) (\mathbf{T}_i^{(-1)} - \mathbf{I}) \left(\prod_{j=i-1}^1 (\mathbf{T}_j^x)^{-1} \right) \quad (60)$$

$$= \mathbf{I} + \sum_i (x_i - x_i^t) (-1)^x \left(\prod_{j=1}^{i-1} \mathbf{T}_j^x \right) (\mathbf{T}_i^{(-1)} - \mathbf{I}) \left(\prod_{j=i-1}^1 (\mathbf{T}_j^x)^{-1} \right) \quad (61)$$

$$= \mathbf{I} + \sum_i (x_i - x_i^t) (-1)^x \left(\left(\prod_{j=1}^{i-1} \mathbf{T}_j^x \right) \mathbf{T}_i^{(-1)} \left(\prod_{j=i-1}^1 (\mathbf{T}_j^x)^{-1} \right) - \mathbf{I} \right). \quad (62)$$

In Eq. (62), we see that we have the same setting as in the special case where we started with the zero vector. There are positive binary variables $(x_i - x_i^t)(-1)^x \in \{0, 1\}$ that tell us if an entry changed from the last binary vector iterate. The new cycle that we consider can be obtained from the old ones through a conjugation:

$$C_i := \left(\prod_{j=1}^{i-1} \mathbf{T}_j^x \right) \mathbf{T}_i^{(-1)} \left(\prod_{j=i-1}^1 (\mathbf{T}_j^x) \right). \quad (63)$$

Since conjugation does not change the cycle type, C_i have the same order as the T_i . If C_k, C_l are not disjoint and k, l are indices where x^{t+1} differs from x^t then P^{t+1} cannot be a permutation matrix, because in some element in the diagonal we subtract a -2 from the identity matrix in Eq. (56). \square

Proof that the Parametrisation $g(x^t)$ Coincides with the Linearised Parametrisation $g^t(x^t)$

Lemma 5. *Within our setting for permutation matrices if $g^t(x^{t+1})$ is a valid permutation matrix then $g^t(x^{t+1}) = g(x^{t+1})$.*

Proof. The non-linearised parametrisation of the permutation matrices starting from the previous iterate x^t is according to Lemma 2:

$$g^t(x^{t+1}) = \mathbf{P}^{t+1} = \prod_{i=1}^k \mathbf{T}_i^x. \quad (64)$$

Using $\mathbf{T}_i^x = \mathbf{I} + x_i(\mathbf{T}_i - \mathbf{I})$ we obtain

$$\mathbf{P}^{t+1} = \prod_{i=1}^k (\mathbf{I} + x_i^{t+1} (\mathbf{T}_i - \mathbf{I})) = \prod_{i=1}^k (\mathbf{I} + x_i^t (\mathbf{T}_i - \mathbf{I}) + (x_i^{t+1} - x_i^t) (\mathbf{T}_i - \mathbf{I})). \quad (65)$$

If we factor everything out we obtain:

$$\begin{aligned} \mathbf{P}^{t+1} &= \prod_{i=1}^k (\mathbf{I} + x_i^t (\mathbf{T}_i - \mathbf{I})) + \sum_{i=1}^k (x_i^{t+1} - x_i^t) \prod_{j=1}^{i-1} (\mathbf{I} + x_j^t (\mathbf{T}_j - \mathbf{I})) (\mathbf{T}_i - \mathbf{I}) \prod_{j=i+1}^k (\mathbf{I} + x_j^t (\mathbf{T}_j - \mathbf{I})) \\ &+ \text{higher order terms.} \end{aligned} \quad (66)$$

This is exactly the linearised parametrisation plus some higher order terms

$$\mathbf{P}^{t+1} = \mathbf{P}(x^t) + \langle \nabla \mathbf{P}(x^t), x^{t+1} - x^t \rangle + \text{higher order terms.} \quad (67)$$

Since we are in a setting where \mathbf{P}^{t+1} is a permutation matrix we can make use of Lemma 4. For 2-cycles this states that if m, l are both indices where x^t differs from x^t then

$$\left(\left(\prod_{j=1}^{m-1} \mathbf{T}_j^x \right) \mathbf{T}_m^{(-1)} \left(\prod_{j=m-1}^1 (\mathbf{T}_j^x)^{-1} \right) - \mathbf{I} \right) \left(\left(\prod_{j=1}^{l-1} \mathbf{T}_j^x \right) \mathbf{T}_l^{(-1)} \left(\prod_{j=l-1}^1 (\mathbf{T}_j^x) \right) - \mathbf{I} \right) = \mathbf{0}. \quad (68)$$

The expression on the left side can be further simplified to

$$\begin{aligned} &\left(\prod_{j=1}^{m-1} \mathbf{T}_j^x \right) (\mathbf{T}_m^{(-1)} - \mathbf{I}) \left(\prod_{j=m-1}^1 (\mathbf{T}_j^x)^{-1} \right) \left(\prod_{j=1}^{l-1} \mathbf{T}_j^x \right) (\mathbf{T}_l^{(-1)} - \mathbf{I}) \left(\prod_{j=l-1}^1 (\mathbf{T}_j^x)^{-1} \right) \\ &= \left(\prod_{j=1}^{m-1} \mathbf{T}_j^x \right) (\mathbf{T}_m^{(-1)} - \mathbf{I}) \left(\prod_{j=m}^{l-1} \mathbf{T}_j^x \right) (\mathbf{T}_l^{(-1)} - \mathbf{I}) \left(\prod_{j=l-1}^1 (\mathbf{T}_j^x)^{-1} \right) = \mathbf{0}, \end{aligned} \quad (69)$$

assuming $l > m$. Inverting all valid permutation matrices that are multiplied to the expression from the right or left side yields the equivalent equation

$$(\mathbf{T}_m^{(-1)} - \mathbf{I}) \left(\prod_{j=m}^{l-1} \mathbf{T}_j^x \right) (\mathbf{T}_l^{(-1)} - \mathbf{I}) = \mathbf{0}. \quad (70)$$

Finally, 2-cycles are their own inverse and

$$(\mathbf{T}_m - \mathbf{I}) \left(\prod_{j=m}^{l-1} \mathbf{T}_j^x \right) (\mathbf{T}_l - \mathbf{I}) = \mathbf{0} \quad (71)$$

will result in terms of higher order in x^{l+1} vanishing.

□

D. Quadratic Assignment

Details on QAPLIB results. We provide further details on the QAPLIB experiment from the main text. The number of instances per problem size is provided in Tab. II.

For a better inspection of the results in Fig. 2, we have sorted them by problem instances, which we display in Tab. III. It is clear that on most instances, our method achieves the best results among the considered benchmark methods. Noteworthy is that we could find optimal solutions on esc problem instances.

n	12	14	15	16	17	18	20	21	22	24
# Instances	8	2	8	13	2	4	8	1	3	1
n	25	26	27	28	30	32	35	40	50	
# Instances	3	8	1	1	2	3	2	1	1	

Table II. QAPLIB [15] problem sizes n used in our experiments.

Iterative Local Search. Because our algorithm only approximates the feasible set, some feasible solutions cannot be accessed by solving the sub-problems, which results in the fact that the algorithm may not find the absolute minimiser. We investigate the impact of iterative local search, which consists of applying some random perturbation on the actual iterate to get rid of local minima. First, we consider multiple restarts of the algorithm with a randomly chosen starting point. The returned solution is the one with the lowest energy over the multiple restarts. Second, we add some noise to the iterate x^t by randomly selecting one of its entries and flipping it. This has the effect that the objective function does not monotonically decrease any more but sometimes oscillates. The returned solution is that with the lowest energy over the iterations.

Table IV summarizes our results on 15 selected challenging QAPLIB problem instances [75]. The single restart version with noisy iterates performs better than the compared versions. In practice, increasing the variance of the noise, that is, the number of iterate entries getting flipped, did not improve the results that much, and a variance set too large makes the algorithm diverge.

E. Shape Matching

Failure Cases on FAUST [10]. We present failure cases of the shape matching experiment in Fig. I. Both Q-Match and our method difficulty register shapes with large pose differences. In particular, they cannot fix left and right, front and back vertices flip of the initial linear assignment.

Experiments on TOSCA Dataset. We perform an experiment on the TOSCA dataset [13]. We register all instances of the cat and dog classes from the dataset.

In the inter-class registration, the source is a cat shape and the targets are dog shapes. Some qualitative results, in line with FAUST results, are presented in Figs. IIa and IIb. On the TOSCA dataset also the methods are non-robust to symmetry flips. We observed failure cases where left and right (e.g. left paw registered to right one), front and back (e.g. tail registered to head), were flipped, and vice versa.

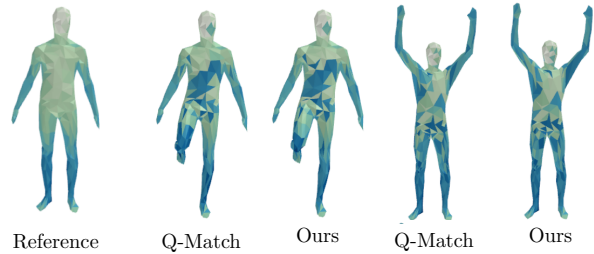


Figure I. Failure shape matching results on the FAUST dataset. The methods partially flip left and right, front and back vertices. This particularly happens on shapes with substantial pose differences.

F. Point Set Registration on D-Wave

We performed point-set registration on D-Wave’s quantum annealer (precisely on the Advantage system, see Sec. 7.4 for the specifics) for $n = 3, 5, 7, 10$ points per set. Our results are reported in Fig. III. Up to $n = 5$ and occasionally for $n = 7$, the quantum annealer is able to successfully register the points, and show more difficulties for larger n .

	nug12	nug14	nug15	nug16a	nug16b	nug17	nug18	nug20	nug21	nug22	nug24	nug25	nug27	nug28	nug30
Optimal	578	1014	1150	1610	1240	1732	1930	2570	2438	3596	3488	3744	5234	5166	6124
Ours	612	1048	1196	1676	1262	1758	1992	2614	2554	3678	3504	3802	5368	5336	6222
Q-Match	608	1028	1182	1640	1264	1816	2014	2650	2574	3682	3608	3966	5486	5342	6408
FAQ	596	1054	1186	1660	1282	1742	1946	2604	2580	3632	3500	3770	5326	5284	6230
2-OPT	620	1040	1216	1704	1288	1870	2004	2738	2526	3842	3658	3866	5544	5316	6416

(a) Results on QAPLIB instances in Ref. [57].

	chr12c	chr12b	chr12a	chr15c	chr15a	chr15b	chr18a	chr18b	chr20c	chr20b	chr20a	chr22b	chr22a	chr25a
Optimal	11156	9742	9552	9504	9896	7990	11098	1534	14142	2298	2192	6194	6156	3796
Ours	12978	11978	10214	13194	13486	10152	15338	1534	16288	2446	2456	6510	6376	4796
Q-Match	13846	11768	9916	12646	12206	11466	14466	1574	25736	3202	3026	6838	6880	4690
FAQ	13088	10468	33082	16884	19852	9112	15440	1712	19836	3206	3166	8582	8920	6744
2-OPT	14636	16748	11370	18634	14234	9404	20960	1710	28800	3616	3918	6810	7114	5502

(b) Results on QAPLIB instances in Ref. [17].

	rou12	rou15	esc16h	esc16i	esc16b	esc16c	esc16d	esc16j	esc16e	esc16a	esc16f	esc16g	rou20	esc32e	esc32g
Optimal	235528	354210	996	14	292	160	16	8	28	68	0	26	725522	2	6
Ours	246244	368728	996	14	292	160	16	8	28	68	0	26	740520	2	6
Q-Match	241844	382094	996	14	292	160	16	8	28	68	0	26	762868	2	6
FAQ	245168	371458	1518	14	320	168	62	8	30	70	0	30	743884	2	10
2-OPT	242552	369238	996	14	292	162	16	12	30	68	0	36	785088	2	6

(c) Results on QAPLIB instances in Ref. [26, 66].

	tai12a	had12	had14	tai15b	tai15a	had16	tai17a	had18	tai20a	had20	tai25a	tai30a	tai35a	tai35b	tai40a
Optimal	224416	1652	2724	51765268	388214	3720	491812	5358	703482	6922	1167256	1818146	2422002	283315445	3139370
Ours	230704	1674	2730	51884360	402384	3740	512198	5432	730642	7004	1222504	1874474	2514120	296071765	3257058
Q-Match	233040	1672	2764	52057859	404700	3720	507218	5400	742112	6930	1222290	1891140	2567762	287049669	3291870
FAQ	244672	1674	2724	52028170	397376	3736	520696	5416	736140	6980	1219484	1858536	2460940	306237113	3227612
2-OPT	246310	1694	2742	51934163	412300	3750	523148	5394	728652	7016	1216938	1888344	2525772	305864564	3340968

(d) Results on QAPLIB instances in Ref. [34, 72, 73].

	scr12	scr15	scr20	bur26f	bur26a	bur26d	bur26h	bur26g	bur26e	bur26b	bur26c	kra32	wil50
Optimal	31410	51140	110030	3782044	5426670	3821225	7098658	10117172	5386879	3817852	5426795	88700	48816
Ours	32696	54926	111286	3807270	5446264	3821372	7131335	10143927	5388824	3825928	5430040	90860	49272
Q-Match	32758	54684	120824	3815606	5444250	3836955	7099875	10121633	5399286	3843293	5427426	94760	49900
FAQ	40758	53114	127150	3784562	5436776	3822209	7121503	10142604	5398837	3827015	5435069	92930	49126
2-OPT	31884	57134	118994	3793300	5445951	3823900	7145161	10121687	5433798	3844335	5442586	94360	49194

(e) Results on QAPLIB instances in Ref. [14, 42, 67, 76].

Table III. QAP results on the QAPLIB dataset sorted by instances. The optimal solution and the best solution among the four benchmark methods in rendered in bold. Our method achieves the best solution most frequently on several problem instances: “chr”, “esc”, “tai” and “bur”. In particular, we also achieve optimal solutions on “esc” problem instances. As reported in Ref. [6], Q-Match performs particularly well on “esc” and “had” instances.

G. Annealing and Embedding on D-Wave

Annealing Process on D-Wave. Programming on D-Wave machines requires defining couplers and biases of the problem and sending them to a quantum processing system. The quantum processor creates a network of logical variables according to the problem size, which is minor-embedded in the quantum hardware. The network starts in a global superposition of all possible basis states. During the quantum annealing, the provided couplers and biases are changed into magnetic fields that deform the state landscape, emphasising the state that is most likely the solution to the underlying optimisation problem.

Minor Embedding. In most cases, our problems result in fully connected logical variables graphs. Embedding of the logical problem onto the quantum hardware often faces the sparse variable connectivity problem. In order to create non-existing physical connections, the QPU *chains* a set of physical variables by setting the strength of their connecting couplers high enough to correlate them.

Fig. IV displays the the embedding on D-Wave of QAP for $n = 5, 10, 15$, as well as the histograms of the sampled energies. Images are obtained from the D-Wave Leap problem inspector. For small n , the histogram looks like a Boltzmann distribution concentrated around the lowest energy. This indicates the confidence of the annealer in the solution

#	Problem	Optimal	Number of restarts		
			50 w/o noise	1 with noise	1 w/o noise
1	chr12c	11156	11566	12470	11566
2	rou12	235528	240664	238954	245208
3	tai15a	388214	393476	400892	394642
4	chr15a	9896	11052	11562	12682
5	chr15c	9504	11758	12980	11212
6	rou15	354210	367812	364192	373132
7	esc16b	292	292	292	292
8	tai17a	491812	503140	508222	509066
9	rou20	725522	746180	734720	751658
10	chr20b	2298	2688	2764	2518
11	tai20a	703482	738124	733400	740484
12	chr22b	6194	6828	6506	6518
13	tai30a	1818146	1896112	1887748	1879078
14	tai35a	2422002	2537102	2483626	2524962
15	tai40a	3139370	3277944	3264446	3277034

Table IV. Randomness analysis of our algorithm on a 15 selected QAPLIB problems. The two digits in the problem’s name stand for the problem size n . Compared are three variants of the algorithm: “50 w/o noise” refers to 50 restarts of the algorithm with different, random starting points and no noise added to the iterates; “1 with noise” refers to a single restart of the algorithm with $x^0 = \mathbf{0}$ and noise added to the iterates; and “1 w/o noise” refers to the standard, single restart of the algorithm with $x^0 = \mathbf{0}$ and no noise added to the iterates. The optimal solution and the best solution among the benchmark variants are rendered in bold. The “50 w/o noise” variant of the algorithm performs only slightly better than the standard run, returning five times the lowest energy compared to four for the standard version. On the other hand, a single restart with noise added to the iterates often performs better than the two other alternatives, returning $8\times$ the lowest energy.

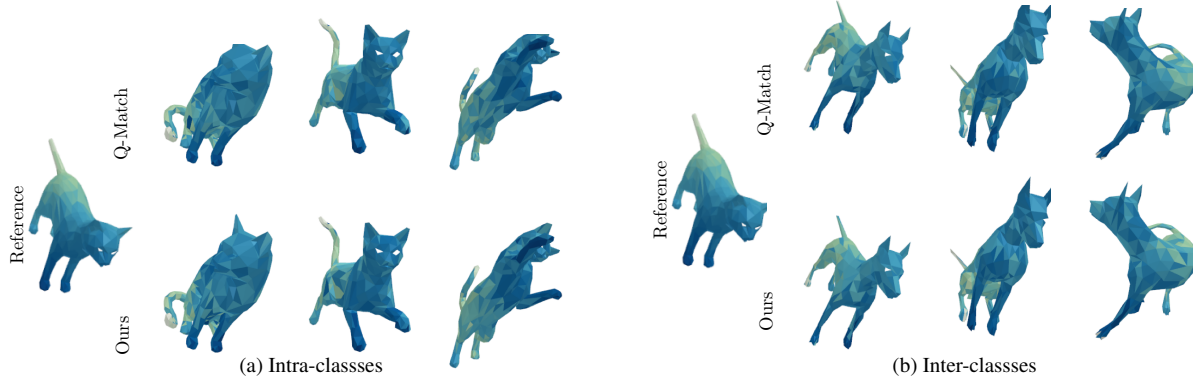


Figure II. Shape matching registration results on the TOSCA dataset [13].

proposal. For larger n , the histogram is uniformly distributed over several different energy values. This is principally due to long chains, which result in chain breakages. When this happens, the several physical variables in the chain, supposed to represent the same logical variable, get discordant spin configurations, which disturb the overall energy of the system. We tried setting the chain strength higher to avoid chain breakages. While this successfully eliminates chain breakages, we observed that it worsened the overall result of the algorithm.

Fig. V presents, for QAP problem instances, the growth of the number of logical and physically allocated variables as a function of the problem size n . The number of allocated physical variables is about ten times the number of logical variables.

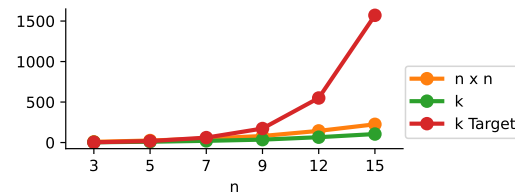


Figure V. Comparing the problem dimension $n \times n$, the number of logical variable $k = n(n - 1)/2$ of our problem modelling and the number of corresponding target variables “ k Target” allocated on the D-Wave machine for different n on QAP.

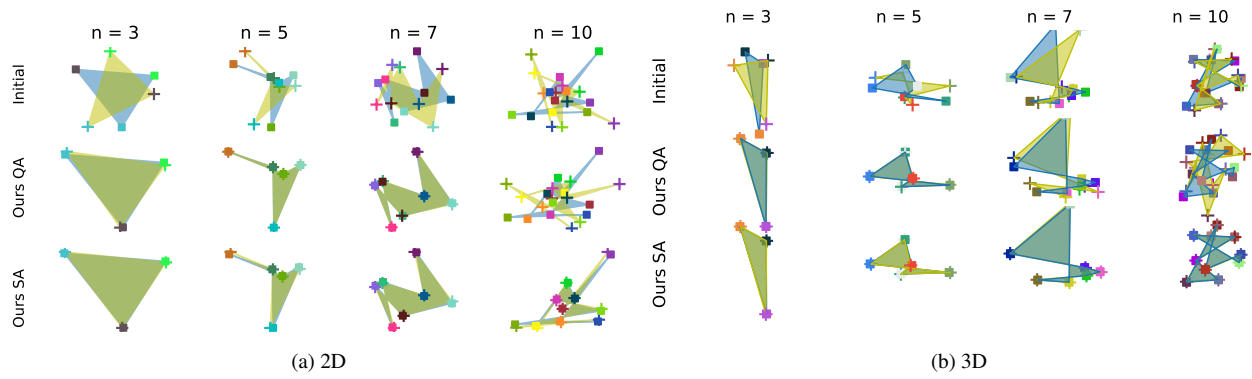


Figure III. Point set registration results computed on D-Wave. Shaded shapes were added for visualisation purposes only. Corresponding points have the same colours, while reference points are marked by squares and template points by crosses. The quantum annealer can register up to $n = 5$ points. From $n = 7$, the quantum annealer can partially recover correct point assignments but fails to perfectly register the points.

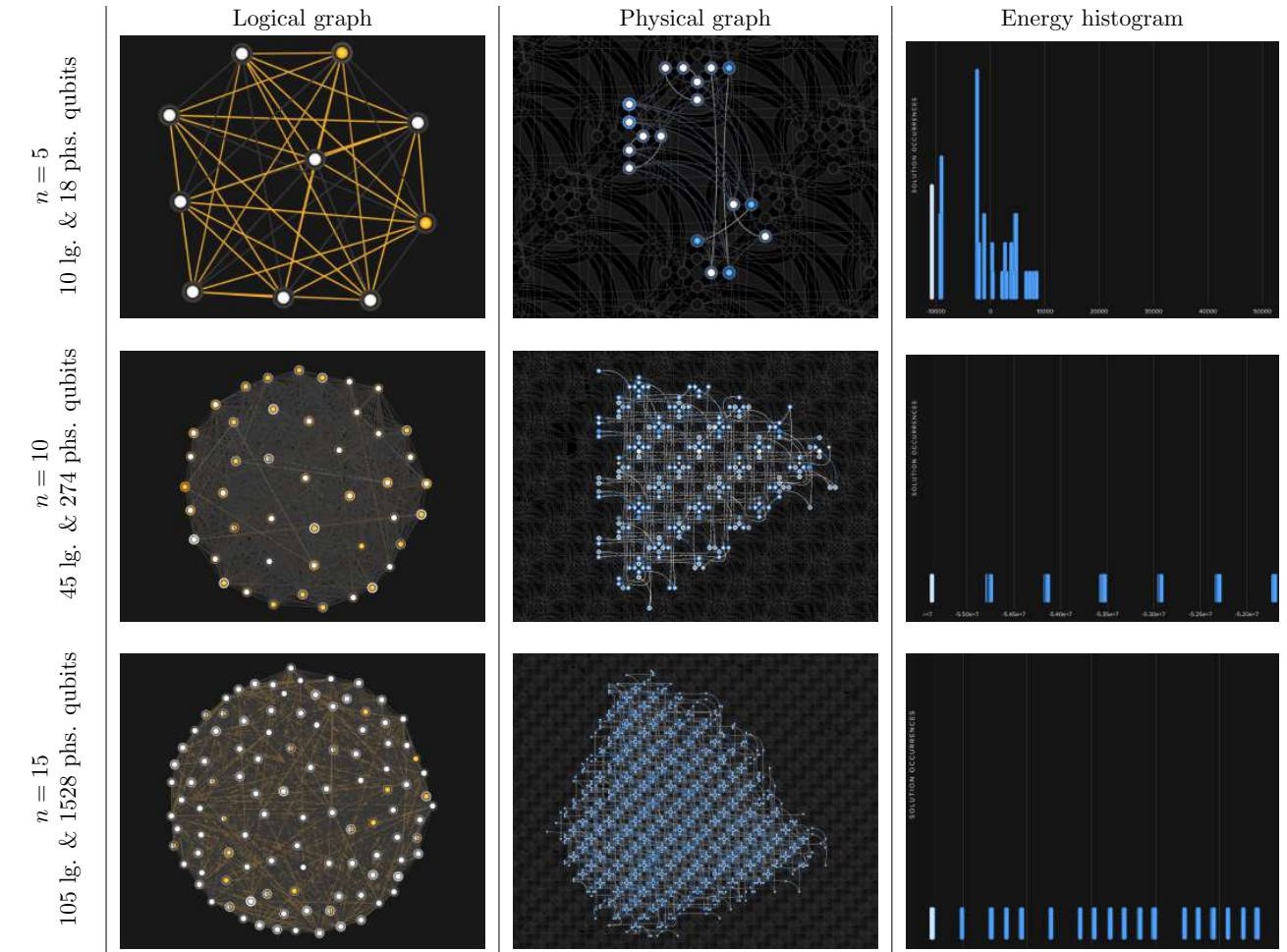


Figure IV. Minor embeddings of QAP on D-Wave for $n = 5, 10$ and 15 . The first column shows the logical graph of the problem, the second one visualises the physical embedding of the logical graph, and the third one is the histogram of the returned samples.